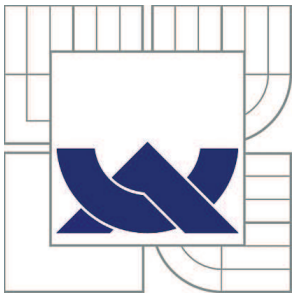

VYSOKÉ UČENÍ TECHNICKÉ V BRNĚ

BRNO UNIVERSITY OF TECHNOLOGY

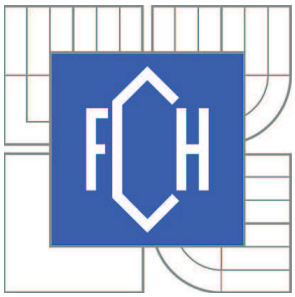

FAKULTA CHEMICKÁ
ÚSTAV CHEMIE POTRAVIN A BIOTECHNOLOGIÍ

FACULTY OF CHEMISTRY
INSTITUTE OF FOOD SCIENCE AND BIOTECHNOLOGY

PARTIAL SLIP IN LIQUIDS STUDIED WITH HIGH-FREQUENCY SHEAR OSCILLATIONS

STUDIUM PARCIÁLNÍHO SKLUZU V KAPALINÁCH S VYUŽITÍM VYSOKOFREKVENČNÍCH STŘIŽNÝCH KMITŮ

DIPLOMOVÁ PRÁCE
MASTER'S THESIS

AUTOR PRÁCE — Bc. JANA VLACHOVÁ
AUTHOR

VEDOUCÍ PRÁCE — Prof. Dr. Diethelm Johannsmann
SUPERVISOR

BRNO 2014

Brno University of Technology
Faculty of Chemistry
Purkyňova 464/118, 61200 Brno 12

Master's thesis Assignment

Number of master's thesis:	**FCH-DIP0842/2013**	Academic year:	**2013/2014**
Institute:	Institute of Food Science and Biotechnology		
Student:	**Bc. Jana Vlachová**		
Study programme:	Chemistry and Technology of Foodstuff (N2901)		
Study field:	Food Science and Biotechnology (2901T010)		
Head of thesis:	**Prof. Dr. Diethelm Johannsmann**		
Supervisors:	prof. Ing. Ladislav Omelka, DrSc.		

Title of master's thesis:

Partial slip in liquids studied with high-frequency shear oscillations

Master's thesis assignment:

1 . Work out a literary summary considering the issue studied
2 . Describe the evaluation methods used
3 . Process the results of the experiments measured
4 . Evaluate the results in the form of a discussion

Deadline for master's thesis delivery: 9.5.2014

Master's thesis is necessary to deliver to a secreatry of institute in number of copies set by dean and in an electronic way to a head of master's thesis. This assignment is enclosure of master's thesis.

Bc. Jana Vlachová Student	Prof. Dr. Diethelm Johannsmann Head of thesis	doc. Ing. Jiřina Omelková, CSc. Head of department

In Brno, 31.1.2014

prof. Ing. Jaromír Havlica, DrSc.
Dean

ABSTRACT

The sphere-plate contact under normal and tangential load in water was studied. As a source of shear oscillation the acoustic resonator (a quartz crystal microbalance - QCM) was used. The contact of a sphere with the surface of resonator induces a shift of resonance frequency and bandwidth. The dependence of the frequency shift Δf and bandwidth shift $\Delta\Gamma$ on the amplitude of oscillation were measured. With increasing amplitude, a decrease in Δf and an increase in $\Delta\Gamma$ were observed. This behaviour is characteristic for partial slip. Applying the Cattaneo-Mindlin model, the contact radius and the friction coefficient were calculated. The contact radius in the limit of small amplitudes increases with increasing normal load. For this dependency, the data fit well to the JKR model. The friction coefficient is of the order of unity, as it should be. It slightly decreases with increasing external normal force, which can be explained with an adhesive force contributing to the total normal force. The formalism yields two separate values for friction coefficient, the first is derived from the frequency shift and the second is derived from the shift in bandwidth. These two values agree with each other within ± 20 % for experiments in liquids, while they differ by about a factor of two for experiments with hydrophilic surfaces in air. This is tentatively explained with capillary forces. The discrepancy points to a shortcoming of the Cattaneo-Mindlin theory.

KEY WORDS

contact mechanics
sphere-plate contact
partial slip, microslip
quartz crystal microbalance (QCM)
Cattaneo-Mindlin model
JKR model

ABSTRAKT

Byl studován kontakt mezi koulí a deskou pod tangenciálním zatížením ve vodě. Jako zdroj střižných kmitů byl použit akustický rezonátor (křemíkové mikrováhy – QCM). Kontakt koule s povrchem resonátoru indukuje změnu resonanční frekvence a šířky pásma. Byla měřena změna frekvence Δf a změna šířky pásma $\Delta\Gamma$ v závislosti na amplitudě oscilací. S rostoucí amplitudou docházelo k poklesu Δf a růstem $\Delta\Gamma$, což je chování typické pro parciální skluz. Díky aplikaci Cattaneo-Mindlinova modelu byl vypočítán kontaktní poloměr a třecí koeficient. Kontaktní poloměr při nízké amplitudě stoupal při zvětšujícím se normálovým zatížením. Tato závislost se dobře shodovala s JKR modelem. Třecí koeficient se nacházel v odpovídajícím rozsahu. Při zvyšování externí normálové síly, docházelo k nepatrnému snižování hodnoty třecího koeficientu. Toto chování je vysvětleno příspěvkem adhezivních sil k totální normálové síle. Výpočtem byly získány dva typy třecích koeficientů, první ze změny frekvence Δf a druhý ze změny šířky pásma $\Delta\Gamma$. Tyto dvě hodnoty se spolu shodovaly z ± 20 % pro měření prováděná ve vodě, zatímco pro dvě měření prováděných na hydrofilním povrchu ve vzduchu se lišila. Tento nesoulad poukazuje na nedostatek Cattaneo-Mindlinovy teorie a mohl by být vysvětlen přítomností kapilárních sil.

KLÍČOVÁ SLOVA

kontaktní mechanika
kontakt koule s deskou
parciální skluz, mikroskluz
křemíkové mikrováhy (QCM)
Cattaneo-Mindlinův model
JKR model

VLACHOVÁ, J. *Partial slip in liquids studied with high-frequency shear oscillations.* Brno: Brno University of Technology, Faculty of chemistry, 2014. 52 s. Supervisor of master's thesis Prof. Dr. Diethelm Johannsmann.

DECLARATION

I declare that the master's thesis has been worked out by myself and that all the quotations from the used literary sources are accurate and complete. The content of the master's thesis is the property of the Faculty of Chemistry of Brno University of Technology and all commercial uses are allowed only if approved by both the supervisor and the dean of the Faculty of Chemistry, BUT.

……

Student's signature

ACKNOWLEDGEMENT

First of all, I would like to express my gratitude to Prof. Diethelm Johannsmann for his patience, support and great leadership of my master's thesis. I am grateful to my colleague Rebekka König for her advice, friendship, support and time which she gave me. I also thank my consultant Prof. Ladislav Omelka. I would like to acknowledge Brno University of Technology for providing financial resources and Ing. Hana Alexová for the help with organizational aspects of the exchange program.

There are so many great people who gave my support and friendship and who they deserve my greatest thank, notably Katja Pohl and Stefanie Telsemeyer-Schauer. Further, I would also like to thank Andreas Böttcher for help with manufacture of laboratory equipment. My thanks go also to Lisa Lehnecke, Nicole Panzier, Heike Römermann, Arne Langhoff, Lisa Müller, Rebecca Reinhardt, Robert Scherf, Astrid Peschel, Judith Petri, Michael Tölle and to other people at the Institute of Physical Chemistry at TU Clausthal as well as to all my other friends in Clausthal for a very good year.

I am grateful to Dr. Hakan Gür for his proofreading of my thesis.

Last but not least, special thanks go to my family. Without their support, my studies would have not been possible. I am deeply indebted to Petr for all his help, support, tolerance and patience.

CONTENTS

1 INTRODUCTION

Contact mechanics deals with deformation of bodies, stress distribution, adhesion, capillary forces and is close connected with tribology.[1–3] In the last few years, contact mechanics, as well as other technologies, focuses on micro and nano-scale. Studies of micro-contacts has been interesting from engineering point of view as well as for medicine and biotechnology.

In medicine, the contact mechanics was employed for the studies of biotribology of articular cartilage,[4] and in biotechnology, for investigation of microbial tribology of biofilms.[5] Contact mechanics has also found inspiration in nature. For instance, the gecko has microfibrils on its feet. These microfibrils have a strong adhesion force to the surface. As a result of these adhesion, gecko can easily climb the walls made of varied materials. This phenomenon is based on contact splitting, i.e. one large contact is divided into plenty of small contacts.[6] Production of materials with a surface which is capable of presenting reusable dry adhesion could be used in many applications, from tapes up to wall-climbing robots.[7]

In engineering, the contacts under tangential load have been in focus of interest, because the tangential contact is not as well understood as contact under normal load. Nevertheless, the tangential load occurs in many engineering devices which operate under the vibration or rolling, e.g. bearings, where the tangential load leads to friction and fretting wear.[8]

Focus of this thesis was the studies of contacts under tangential load, when transition between stick and slip occurs. In this transition the centre of contact area stick while the edge of contact area slides. This phenomenon is called partial slip and is related to friction, wear and crack propagation.

The aim of the thesis was to answer following questions:

- Does partial slip occur in water?
- Is there any difference between partial slip in water and in air?
- Which of the models for partial slip fit better – Cattaneo-Mindlin or Savkoor?
- Is the condition of equality for friction coefficients $\mu_{\Delta f}$ and $\mu_{\Delta\Gamma}$ fulfilled?
- Which of the models for dependence of contact radius on normal force is in better accordance – Hertz or JKR?
- How is partial slip influenced by particles' size?
- How is partial slip influenced by varied surface?

2 THEORETICAL PART

2.1 Contact mechanics

The description of behaviour of bodies which are in contact is a big field of interest for current engineering. The contact between two bodies causes the stress at the interface between them, which can lead to friction, fretting wear and up to fractures. Contact mechanics uses complex mathematical models for the description of contacts. These models describe contacts between varied bodies such as two spheres, a sphere and a flat surface, two cylinders or a cone and a flat surface, etc. Each of these contacts displays a different shape of contact area. For instance, the contact area of spheres-sphere contact or sphere-plane contact is a circle, whereas for two cylinders it is a line. This thesis will focus on sphere-plane contact.[1–3]

2.1.1 Non-adhesive contacts – Hertz model

The first publication about contact mechanics was written by Heinrich Hertz in 1882.[9] The Hertz model predicts a behaviour of two elastic bodies which are in normal contact (contact under normal load) but without the influence of adhesive forces and friction.[2]

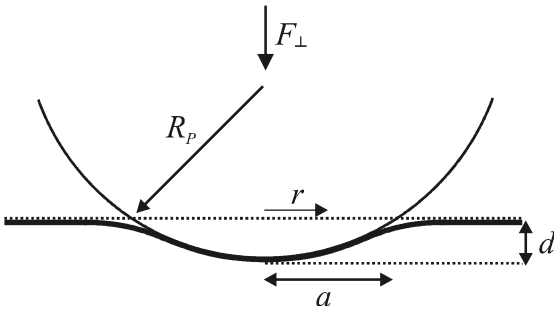

Fig. 1 Hertz contact (drawn according to Ref.[1])

If a rigid sphere with radius R_P is in contact with an elastic flat surface, the contact area forms a circle with the radius a. This contact radius depends on the applied normal force $F_\perp$ and the elastic properties of the material as[1]

$$a = \left(\frac{3F_\perp R_P}{4E^*} \right)^{\frac{1}{3}} \tag{1}$$

where E^* is an effective modulus. This effective modulus combines elastic properties of the two materials. E_1 and ν_1 describe elastic modulus and Poisson's ratio for the sphere and E_2, ν_2 for the material of the surface.[3]

$$\frac{1}{E^*} = \frac{1-\nu_1^2}{E_1} + \frac{1-\nu_2^2}{E_2} \tag{2}$$

The penetration depth d depends on the contact radius as[1]

$$d = \frac{a^2}{R_P}. \tag{3}$$

The distribution of normal stress p is described by the following equation[1]

$$p = p_0 \left(1 - \frac{r^2}{a^2}\right)^{\frac{1}{2}}, \tag{4}$$

where p_0 is the normal stress in the centre of the contact area and r is the distance from this centre. That means that the normal stress on the edges of the contact area goes to zero and the maximal normal stress occurs in the centre of the contact area and is represented by[1]

$$p_0 = \left(\frac{6F_\perp E^{*2}}{\pi^3 R_P^2}\right)^{\frac{1}{3}}. \tag{5}$$

The Hertz model assumes no friction and adhesive force in contact. Yet, this is only true for normal contact of bodies with the same elastic properties because they deform in the same way. For bodies with different elastic properties in normal contact, the relative tangential displacement leads to transverse expansion of the bodies and it causes frictional stress.[1]

2.1.2 Adhesive contacts – JKR model

Adhesive forces are weak forces, short distance interactions between atoms or molecules of bodies, such as van der Waals forces. These forces are very strong between two smooth surfaces. However, real surfaces are not homogenous and adhesive forces are significantly reduced by already-present fractures and roughness of the surface.[1]

The adhesive force between solid bodies was calculated by Bradley in 1932. [10] For bodies in direct contact, the equation has the following form[1]

$$F_{adh} = -4\gamma\pi R_P \tag{6}$$

In the early 1970s, Johnson, Kendall and Roberts modified the Hertz theory and formulated a new model including adhesive forces, called JKR model.[11]

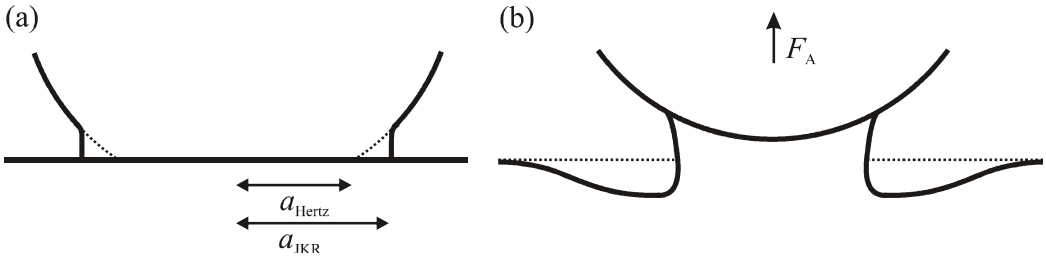

Fig. 2 JKR contact - (a) contact radius (b) pull-off force (drawn according to Ref.[1])

They found out that contacts under high loads correlate with Hertz theory, but contacts under low loads have larger contact radii than Hertz predicted and for separation of bodies a negative load (pull-off force) is needed.[1,11]

$$F_A = -\frac{3}{2}\Delta\gamma\pi R_P \tag{7}$$

$$a = \left(\frac{3R_P}{4E^*}\left(F_\perp + 3\Delta\gamma\pi R_P\right) + \sqrt{6\Delta\gamma\pi R_P F_\perp + \left(3\Delta\gamma\pi R_P\right)^2}\right)^{\frac{1}{3}} \tag{8}$$

where $\Delta\gamma$ is the surface energy. When $\gamma = 0$, then the equation turns into simple Hertz model (equation 1).

Since then varied models of adhesive contact have been described by Derjaguin, Muller and Toporov[12], Tabor[13], Maugis[14], and the like, but these models are beyond the scope of this thesis.

2.1.3 Friction

Friction is a part of everyday life. Friction accompanies walking, driving, writing with a pencil, etc.[15] as well as technological processes using abrasive techniques. Maximum friction is achieved intentionally only in a few cases such as contact between tires and a road during braking. In the majority of cases, mainly in engineering, there is an effort to suppress this friction because it leads to dissipation of energy and causes wear and fractures.[1] Friction was first studied in the Renaissance Period by Leonardo da Vinci. He developed the first friction laws in which the frictional force is proportional to normal force and does not depend on the contact surface.[1,15]

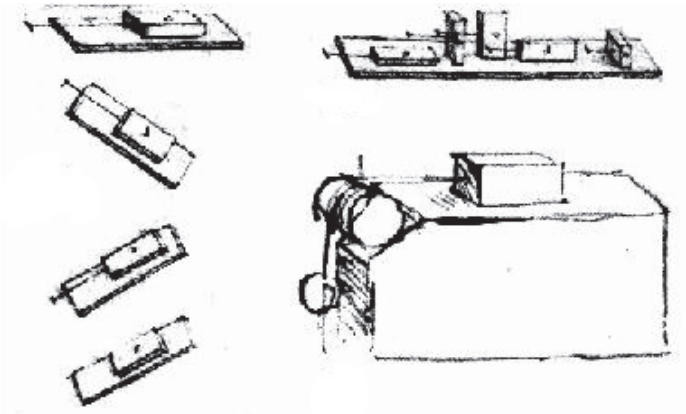

Fig. 3 Leonardo da Vinci's drawing of friction[16]

Over the time this law was forgotten and in 1699 Amontons rediscovered it. It is for this reason that this law is known as Amontons' law. 80 years later, Coulomb verified Amontons' result and defined the difference between static and kinetic friction.[1,15]

Static friction F_s and kinetic friction F_k are given as

$$F_s = \mu_s F_\perp \tag{9}$$

$$F_k = \mu_k F_\perp \tag{10}$$

where μ_s is the static friction coefficient and μ_k is the kinetic friction coefficient. Both friction coefficients are independent of the normal force and the contact area. They depend on the properties of material and μ_s is higher than μ_k.[1,17] In engineering, lubricants are added for decreasing the friction coefficient, thereby the friction and fretting wear are reduced.[18]

The problem of micro-contact under tangential load will be discussed later in chapter 2.3.1.

2.2 Quartz crystal microbalance

Quartz crystal microbalance (QCM) is a mass sensing device which contains an acoustic resonator based on a piezoelectric effect. This resonator is composed of a crystalline quartz disk with two electrodes. The quartz is in α modification.[19]

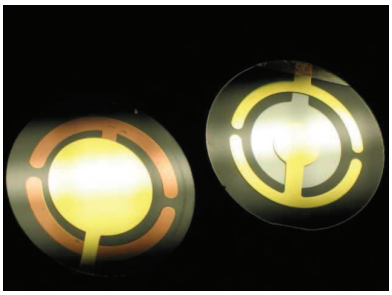

Fig. 4 Quartz crystal microbalance[20]

The piezoelectric effect is a reversible process of electro-mechanical coupling. The alternating electric current passes through the electrodes and causes a mechanical deformation as a result of the piezoelectric properties of the crystal. If the frequency of the alternating field is equal to the resonant frequency of the crystal, resonance occurs. This deformation causes a polarization of the crystal surface. Due to polarization, electric current is generated and can be subsequently detected.[19]

The excited crystal can oscillate in the following modes.

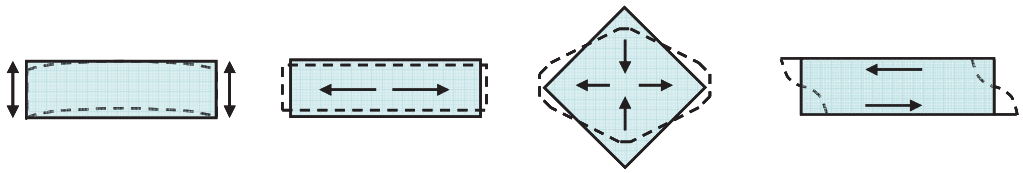

Fig. 5 Oscillation modes of quartz crystal – flexure, extensional, face-shear and thickness shear mode [20]

In this work, AT-cut quartz crystal was used. AT-cut crystal utilizes thickness shear mode of oscillation and its resonance frequency is only slightly influenced by variable temperature.[19]

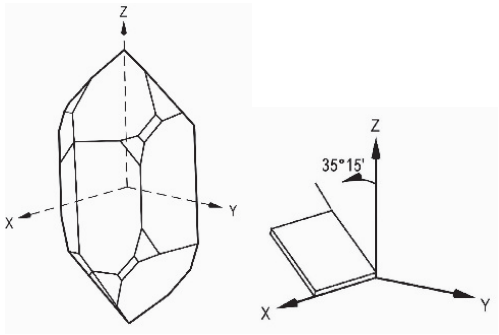

Fig. 6 AT-cut of quartz crystal[21]

The fundamental frequency f_F is determined by the thickness d_q of the crystal.[20]

$$d_q = \frac{\lambda}{2} \tag{11}$$

$$f_F = \frac{c_q}{\lambda} = \frac{c_q}{2d_q} \tag{12}$$

The λ is the wavelength. The c_q is the speed of sound of quartz.

Furthermore, the crystal oscillates at the fundamental frequency and also at other frequencies – so-called harmonics – which are close to the integer multiples of the fundamental frequency. The electrical signal can be measured only for odd harmonics which cause a polarization of the surface. Even harmonics cannot be measured because of their symmetry. Induced charge on crystal surfaces has the same sign and, therefore, the crystal cannot be polarized.[20]

As mentioned above, due to this polarization, electric current is generated. With impedance analysis, one can measure the conductance which is a function of frequency. The conductance curve is fitted with a resonance curve. Among the fit parameters which characterize the resonance are frequency f and bandwidth Γ. The bandwidth Γ terms half-width at half-maximum of the resonance frequency and is used for quantification of energy dissipation.[22]

2.2.1 Measurement of thickness of films with QCM

As described in the previous chapter, the resonance frequency is inversely proportional to the thickness of the crystal. When the crystal surface is coated with polymer layer, then the resonance frequency is shifted to lower values because the wave travels extended distances through the crystal. The models, which describe this behaviour differ in terms of the kind of deposited layer.

In 1959 Sauerbrey published a paper where he described the effect of thin rigid layers deposited on QCM. Sauerbrey observed that the shift of frequency to lower values is directly proportional to the mass of film m_f (equation 13) and determines measurable limit of QCM up to 10^{-10} kg.[20,23] QCM has become a very sensitive weighing method and hence it is called microbalance. The frequency shift and the deposited mass are related as

$$\Delta f = -m_f \frac{2n \cdot f_F^2}{A_{eff} Z_q} \tag{13}$$

The n is the order of overtone, $A_{eff} = 33 \cdot 10^{-6}$ m^2 is an effective area and $Z_q = 8.8 \cdot 10^6$ kg·m^{-2}·s^{-1} is an acoustic impedance of the quartz. If the density of deposited film ρ_f is known, the thickness of the layer can be calculated as[24]

$$\Delta d = -\frac{Z_q \cdot \Delta f}{2n \cdot f_F^2 \cdot \rho_f} \tag{14}$$

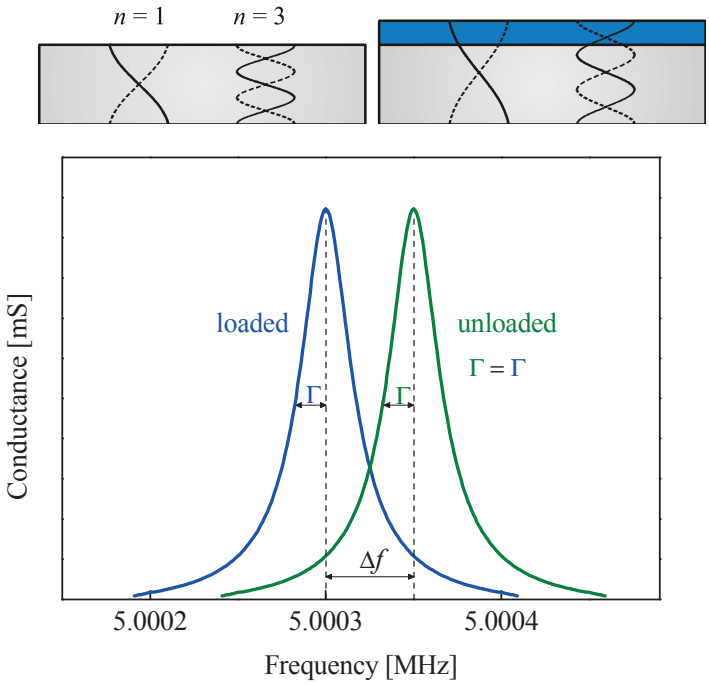

Fig. 7 Sauerbrey model (drawn according to Ref. [20])

Further, Kanazawa et al. described a model for liquids and viscoelastic layers. In this model, the resonance frequency shifts towards lower values for frequencies as for Sauerbrey's rigid layer. However, bandwidth increases because of large energy dissipation.[25,26]

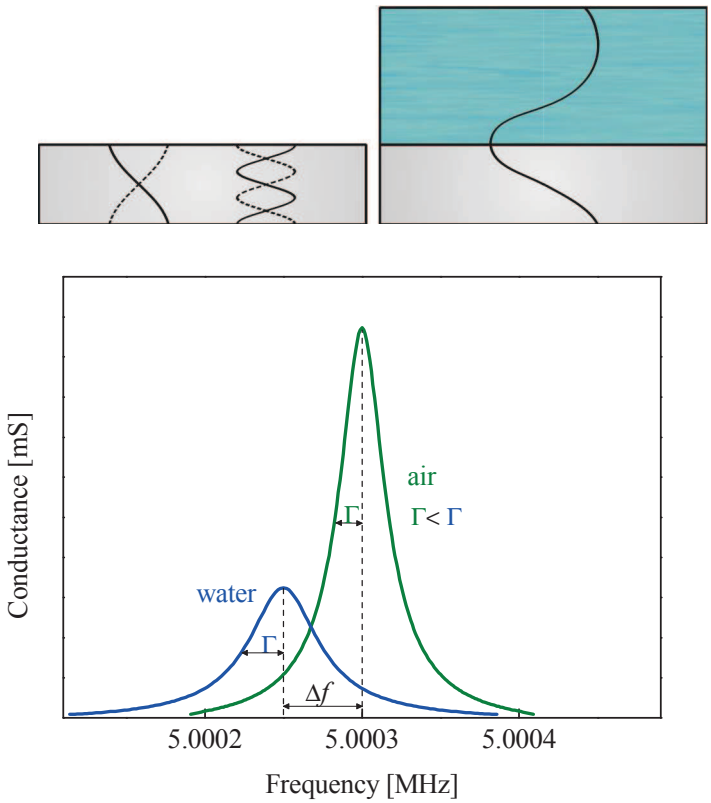

Fig. 8 Kanazawa model (drawn according to figure created by Rebekka König and Ref.[24])

2.2.2 QCM as a biosensor

The high accuracy of weighing of QCM is mainly used to measure the adsorption of molecules on the surface. This is widely employed in biotechnology. QCM is used for studies of all kinds of biomolecules immobilization and interactions e.g. protein-protein, protein-carbohyrdate, protein-oligonucleotide, enzyme activity, small molecule-receptor interaction, etc. Further QCM can be used for detection of bacteria, studies of cell, their attachment, adhesion, proliferation or forming of biofilm. QCM has become a powerful bioanalytical tool for the last few years.[27]

2.3 Measurement of contact mechanics with QCM

QCM is widely used for measuring the thickness of applied layers. Nevertheless it is also possible to measure the behaviour of contacts. There are two phenomena. The first is for small particles (size under 50 μm) tightly attached to the crystal. In this case this particle increases the mass of the resonator, thereby the resonance frequency decreases according to Sauerbrey's equation.[28]

The second phenomenon was observed by Dybwad in the mid-1980s for large spheres. Dybwad observed that for contact of these particles with the surface of the resonator, the resonance frequency was shifted to higher values. He explained this phenomenon as a mechanical model of coupled resonators. The behaviour of the resonance frequency corresponds with the behaviour of spring, which is characterized by a spring constant. The spring constant is also called contact stiffness κ. The heavy particle is held in place by inertia. With a tangential force (crystal oscillation) applied, the particle exerts the restoring force, which causes an increase in the stiffness of the coupled resonators and this leads to an increase in resonance frequency.[29]

Increase in bandwidth is caused by energy dissipation, because the acoustic wave radiates into the sphere. This radiation can be depicted in the mechanical model by adding a dashpot parallel to the spring.[28]

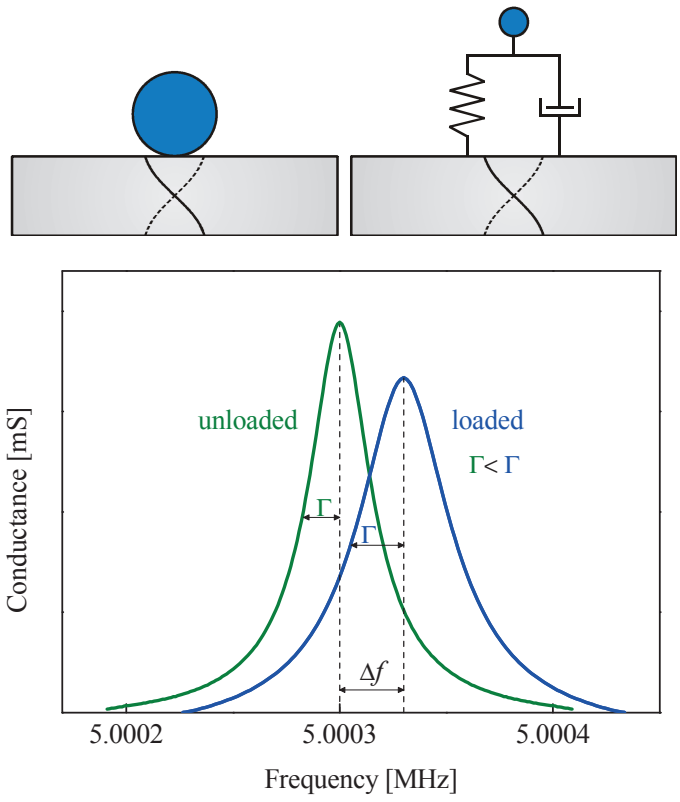

Fig. 9 Dybwad model (drawn according to Ref.[20])

In this thesis, the model of Small Load Approximation (SLA) is used for the description of changes in frequency and bandwidth caused by stress on the quartz surface. It is possible to use SLA for each linear model described above and also for nonlinear behaviour – which will be described below – if the change in frequency is much smaller than fundamental frequency. [20] SLA model will not be discussed in detail because it is beyond the scope of this thesis. For a detailed description of SLA see Ref.[22].

2.3.1 Partial slip

Previous models are based on absolutely smooth and frictionless contact. Upon contact of two bodies under tangential load, tangential stress must be taken into account.[1]

At first, the contact under tangential load without sliding will be described. If these bodies tightly adhere – for instance, when they are glued together – there is no sliding between them under tangential displacement. The stress distribution is depicted in Fig. 10. The normal stress $\sigma_\perp$ is maximal in the centre of contact area, and towards edges approaches zero like in Hertz model (chapter 2.1.1). Yet, as a consequence of tangential load, tangential stress $\sigma_\parallel$ at the edges of contact area goes to infinity.[1]

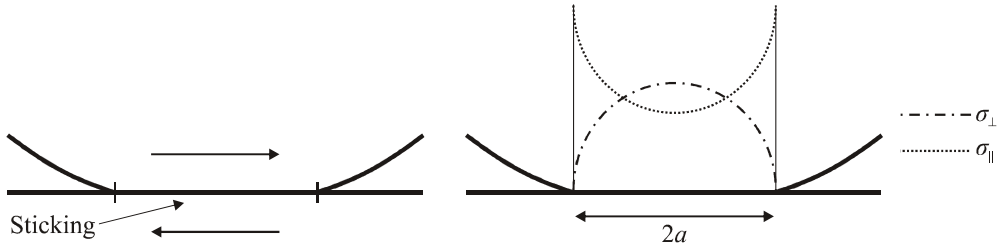

Fig. 10 Tangential contact without slip - stress distribution (drawn according to Ref.[1])

The stiffness of contact κ is given as [1]

$$\kappa = 2G^* a\,, \tag{15}$$

where G^* is an effective shear modulus. This modulus is a combination of elastic properties G_1, G_2, ν_1 and ν_2 of two elastic bodies, and is given as[1]

$$\frac{1}{G^*} = \frac{2-\nu_1}{4G_1} + \frac{2-\nu_2}{4G_2}\,. \tag{16}$$

The shear modulus G is related to extensional modulus E by the following equation[1]

$$G = \frac{E}{2(1+\nu)} \tag{17}$$

Contacts which do not stick together so tightly undergo sliding at the edges of contact area, while the centre of contact sticks in the same place. This phenomenon is called partial slip or microslip.[1]

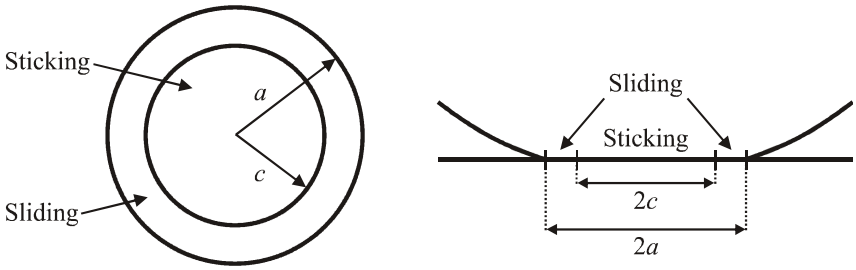

Fig. 11 Sticking and sliding zone in tangential contact (drawn according to Ref.[1])

There are two different theories which describe partial slip – Cattaneo-Mindlin model[30] and Savkoor's model.[31] Cattaneo-Mindlin model assumes standard macroscopic friction in the sliding zone (equation 10). It means the tangential stress $\sigma_{\parallel}$ is proportional to normal stress $\sigma_{\perp}$.[30] |

$$\sigma_{\parallel} = \mu\sigma_{\perp} \tag{18}$$

The stress distribution is a combination of known distributions and is illustrated in Fig. 13a.[1]

Cattaneo-Mindlin model predict tangential displacement of sphere relative to surface as a function of tangential load.[30] In contact mechanics, these force-displacement relations often are nonlinear. The equations 19 and 20, which are derived from CM model, show linear dependence of frequency shift Δf and bandwidth shift $\Delta\Gamma$ on amplitude of quartz oscillation u_0. The connection between force-displacement relations and dependence of Δf and $\Delta\Gamma$ on u_0 is illustrated in Fig. 12. Δf is proportional to the ratio of tangential force and displacement at the turning point and $\Delta\Gamma$ is proportional to area inside the loop divided by u_0^2.[32]

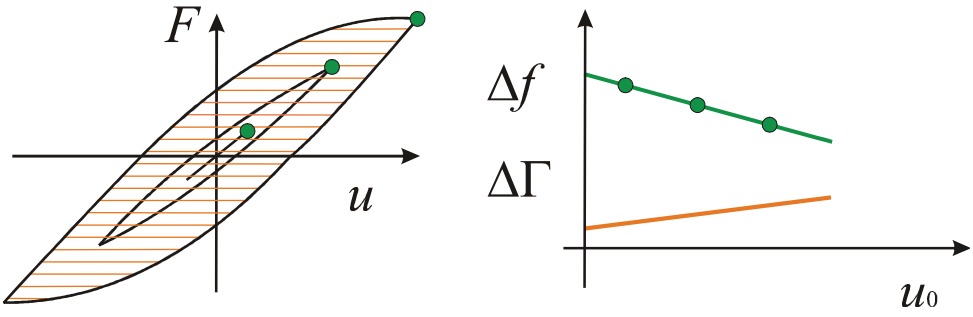

Fig. 12 Force-displacement diagram of partial slip[20]

Equations of this dependence are derived from Cattaneo-Mindlin model.[32]

$$\Delta f(u_0) \approx \frac{n_p}{2n\pi^2 A_{eff} Z_q} \kappa \left(1 - \frac{\kappa}{3\mu F_\perp} u_0\right) \tag{19}$$

$$\Delta\Gamma(u_0) - \Delta\Gamma_{off} \approx \frac{n_p}{2n\pi^2 A_{eff} Z_q} \kappa \left(\frac{4}{9\pi} \frac{\kappa}{\mu F_\perp} u_0\right) \tag{20}$$

n_p is number of spheres, n is the order of overtone, A_{eff} is the effective area and Z_q is the acoustic wave impedance of AT-cut quartz, κ is contact stiffness and μ is friction coefficient. According Cattaneo-Mindlin model the friction coefficient from frequency shift $\mu_{\Delta f}$ should be equal to the friction coefficient from bandwidth shift $\mu_{\Delta\Gamma}$. If the friction coefficient goes to infinity, the partial slip does not occur.[32]

Following equation 15, the Mindlin contact radius of contact area is given as[1]

$$a_{Mindlin} = \frac{\kappa}{2G^*} \tag{21}$$

Savkoor's model assumes constant tangential stress $\sigma_\parallel$ in the sliding zone, which is often obeyed on the micro-scale[31] (Fig. 13b). Equations for frequency and bandwidth shift as a functions of amplitude calculated from Savkoor's model show quadratic dependence[32] (Fig. 14).

$$\Delta f(u_0) \approx \frac{n_p}{2n\pi^2 A_{eff} Z_q} \kappa \left(1 - \frac{5}{8}\left(\frac{\kappa u_0}{4\tau_0 a^2}\right)^2\right) \tag{22}$$

$$\Delta\Gamma(u_0) - \Delta\Gamma_{off} \approx \frac{n_p}{2n\pi^2 A_{eff} Z_q} \kappa \frac{8}{6\pi}\left(\frac{\kappa u_0}{4\tau_0 a^2}\right)^2 \tag{23}$$

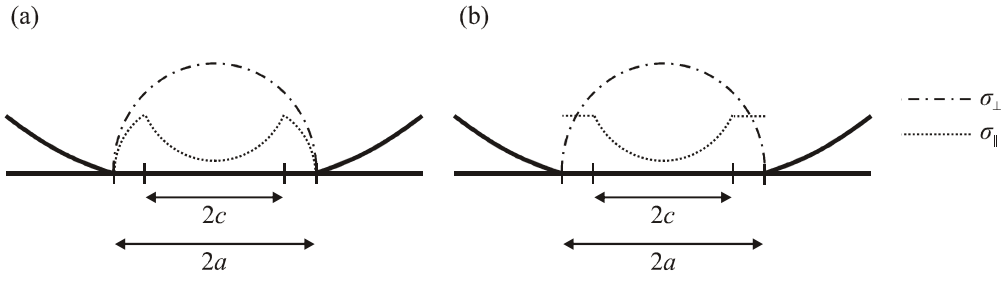

Fig. 13 Stress distribution of partial slip according to (a) Cattaneo-Mindlin and (b) Savkoor (drawn according to Ref.[1, 32])

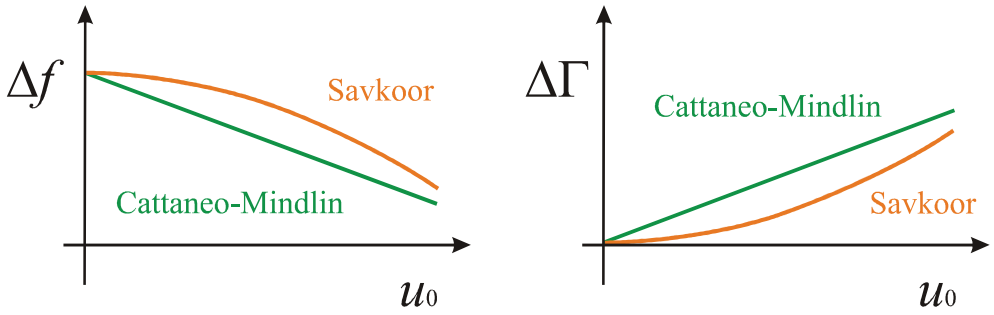

Fig. 14 Difference in dependence of frequency shift and bandwidth shift on amplitude of oscillation between Cattaneo-Mindlin model and Savkoor's model (drawn according to Ref.[32])

2.3.2 Gross slip

With increasing tangential load, the sliding zone of contact expands. At critical points, this expansion leads to sliding of the whole contact. This phenomenon is called gross slip. Fig. 15 shows force-displacement diagram and dependence of Δf and $\Delta\Gamma$ on u_0. At the critical point, $\Delta\Gamma$ decreases, which is denoted as the transition of partial slip to gross slip.[20,32]

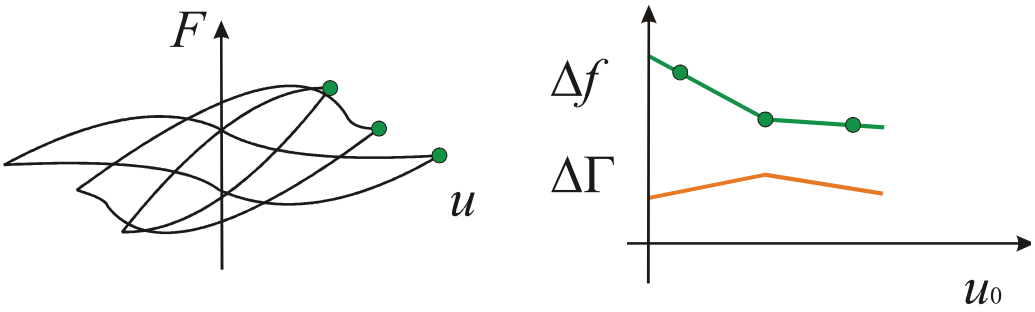

Fig. 15 Force-displacement diagram of gross slip[20]

2.3.3 Viscoelastic contact

For small contacts or larger contacts at small amplitudes, partial slip can be suppressed. These contacts are termed viscoelastic. The behaviour of these contact is linear. The transition of linear behaviour to nonlinear behaviour (partial slip) is characterized by a critical amplitude u_{cr}.[32,33]

Suppression of partial slip for small contacts is interesting in engineering processes because partial slip leads to fretting wear. Due to this, protection against fretting wear could be solved by contact splitting.[32]

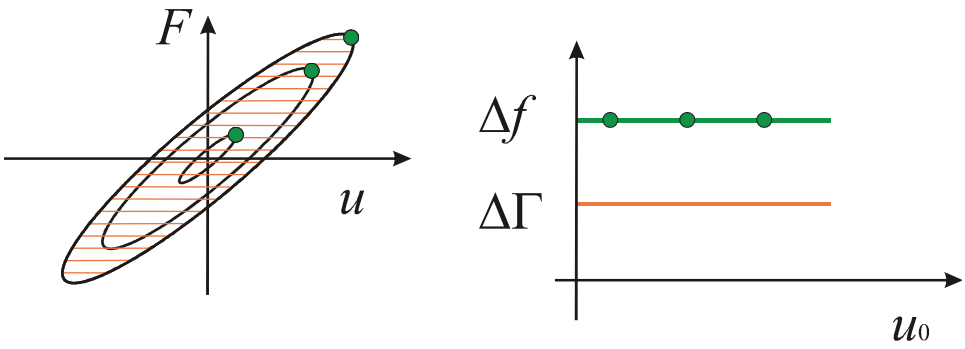

Fig. 16 Force-displacement diagram of viscoelastic contact[20]

2.3.4 Shake-down and shake-up

One reason of apparently nonlinear behaviour of contact is that the contact changes in the time because of aging (temperature, abrasion, etc.).[20]

During periodic plastic deformation, the decrease in energy dissipation after few cycles can be observed.[34] This phenomenon is called shake-dow. In the frictional contact, the shake-down can be a consequence of abrasion caused by repetitive sliding. The frictional forces decrease and due to smoother surface the adhesion is stronger.[1,32] According to these claims, the partial slip should occur only in few loading cycles and after that the contact is stabilized throughout the contact area.[35] The opposite of shake-down is a phenomenon that might be called shake-up where energy dissipation increases during the time[20] (Fig. 17, Fig. 18 and Fig. 19).

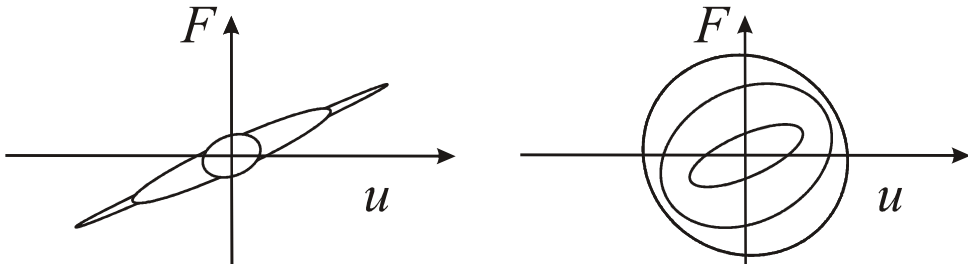

Fig. 17 Force-displacement diagram of shake-down and shake-up[20]

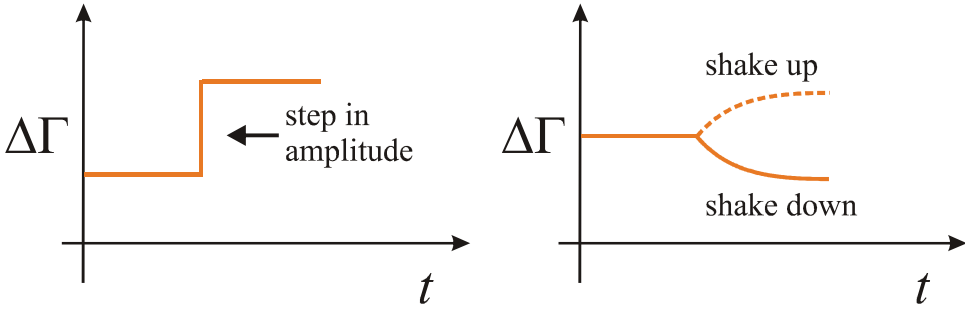

Fig. 18 Bandwidth shift in time after a step in amplitude[20]

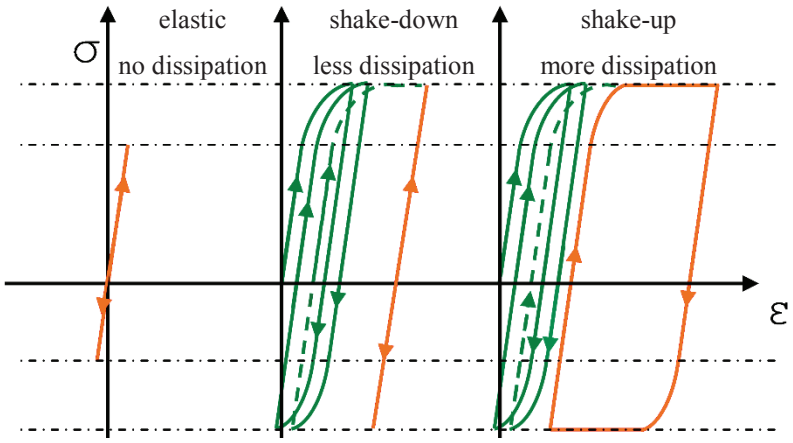

Fig. 19 Stress-strain curves[20]

3 EXPERIMENTAL PART

3.1 Materials and methods

3.1.1 Facilities

Quartz crystal microbalance – parameters:

- 5 MHz
- Thickness 330 μm
- Width 2.54 inch
- Front electrode 13 mm, back electrode 6 mm
- With golden electrodes (unknown)
- With silica surface and titanium electrodes (Maxtec, USA)

Holder – home-built

Humidity and temperature sensor (Testo, AG, Lenzkirch)

Network analyser (Agilent, Malaysia)

Analytical balance (Sartorius, Göttingen)

Spin coater (Laurell, USA)

Stereoscope (Will-Wetzlar, Germany)

UV ozone cleaner (BioForce Nanoscience, USA)

3.1.2 Chemicals

Poly(methyl metacrylate) – PMMA

3.1.3 Other material

Borosilicate spheres (Fischer glass, Germany)

Metal plates – home-build (brass, ∅ 6 mm, 0.5 g per piece)

Superglue (UHU)

3.2 Procedure

The experiment is based on measuring of shift of the resonance frequency Δf and bandwidth $\Delta\Gamma$ which is caused by contact of three spheres with quartz surface. These changes in resonance frequency of QCM are detected by impedance analyser.

3.2.1 Preparation of a plate with spheres

Spheres with a diameter of 2 mm and 1 mm were used. These spheres were glued to the metal plate to prevent rolling around on the crystal surface (Fig. 20).

Various kinds of glues were tried. Finally, the superglue was chosen. The superglue is composed of cyanoacrylate, which polymerizes in presence of water (humidity in air)[36] and is waterproof. Resistance to water is important for the measurement.

Fig. 20 Metal plate with glass particles

3.2.2 Coating of crystal

Two types of crystal coating were used. The first coating was a silica coating. This crystal already displayed this surface modification when it was purchased.

The second type of coating was PMMA. PMMA was prepared by Rebekka König. Glass transition temperature of PMMA was T_g = 99.9 °C (literature value T_g = 104.85 °C, calculated by Fox equation [37]). The solution of PMMA in 2-butanone was used. The solids content of the pure PMMA in solution was around 3 %. This coating was applied to the crystal with gold electrodes by using a spin coater. A drop of PMMA solution was applied on the crystal surface. Coating by spin coater was carried out at 6000 rpm for one minute. Subsequently, the coated crystal was dried in a drier at 110 °C over night. The thickness of PMMA was measured with QCM according to Sauerbrey equation. The thickness of PMMA was around 255 nm.

3.2.3 Improvement of holder

For better reproducibility, a new holder of QCM was created (Fig. 21). This holder keeps particles on the same place and protect against breaking of contact, which is very important for the experiment.

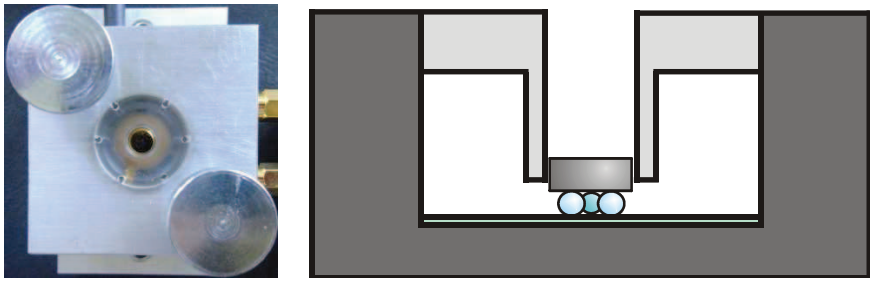

Fig. 21 Improved home-built holder

3.2.4 Experiment performance

The crystal was mounted in the holder. By ramping the applied voltage up and down, the amplitude of oscillation was gradually increased and subsequently decreased (twice). The shift of resonance frequency and bandwidth was determined by impedance analyser. At first, the reference resonance frequency of bare crystal without particles was determined. In the experiments in water, the frequency and bandwidth shift of the crystal covered by water (1 ml) were determined. Subsequently, the plate with particles was placed onto the crystal (Fig. 22). The dependence of frequency and bandwidth shift on amplitude of oscillation was observed. Gradually, for each measurement, the normal force was increased by adding of weight of 0.5 g, 1.0 g, 1.5 g, 2.0 g and 2.5 g. The weight of the plate itself was 0.5 g. This means that the final values of applied mass were from 0.5 g to 3.0 g.

The applied drive level for excitation of amplitude was varied from -15 dBm to +10 dBm, for measurements in air and from -15 dBm to +16 dBm for measurements in water. dBm is a logarithmic scaling of watts, where 0 dBm correspond to 1 mW and 20 dBm correspond to 10 mW.

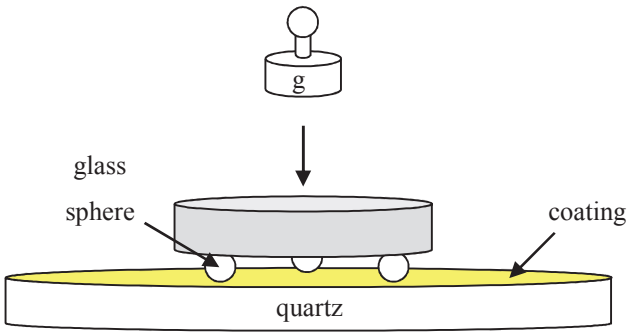

Fig. 22 Scheme of experiment[20]

Experiments were performed under different condition, as shown in Tab. 1. The basic experiment was carried out with particles with a diameter of 2.2 mm in diameter on the silica surface. In the next experiment, the particle size was varied. Also, spheres with a diameter of 1 mm were used on silica surface (in the thesis, the expressions 2 mm particles and 1 mm particles will be used which mean diameter of particles). Finally, the experiment was perform again with 2 mm particles, but on the PMMA.

Tab. 1 Varied conditions

Particle diameter [mm]	Surface	
	SiO_2	PMMA
2.2	air/water	air/water
1.2	air/water	—

3.2.5 Shake down and shake up measurements

The experiments for shake-down and shake-up were performed in the same way as experiments for partial slip, but the Δf and $\Delta\Gamma$ dependent on u_0 were observed over time. In other words, 100 points of Δf and $\Delta\Gamma$ for one amplitude was taken and after the amplitude was changed. This experiment was carried out only with 2 mm spheres on silica surface in air and in water.

4 RESULTS AND DISCUSSION

4.1 Partial slip in water

The fundamental goal of this work was to find out whether the partial slip occurs in water or not. The occurrence of partial slip in water was confirmed and was further studied by other measurements and comparison to the corresponding calculations.

Fig. 23 and Fig. 24 show examples of measurement in air and water. Following the Fig. 12 from chapter 2.3.1, one can find an agreement between results and theory. In air, the partial slip was observed for all types of particles with applied mass around 1.5 - 3.0 g. For smaller loads 0.5 g and 1.0 g, there was a transition from partial slip to gross slip. With the increasing mass, the transition was shifted to the higher amplitude (from 10 nm to 17 nm) up to point of vanishing of these transition. This was expected because, with an increase in normal load, the stiffness increases and the contact becomes more stable. This results correspond with previous results mentioned in Ref.[20].

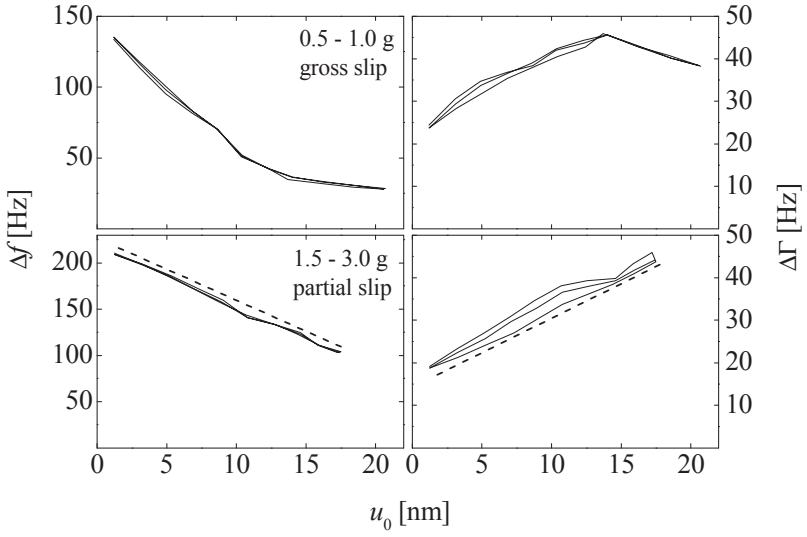

Fig. 23 Measurements in air (2 mm particles on silica surface)

Measurements in water differ from experiments in air. First of all, one can see a big damping caused by water which causes a negative frequency shift and a large increase in bandwidth. This behaviour is predicted by the Kanazawa model (chapter 0). Secondly, there was no gross slip observed in water. This could be also explain as a result of damping. In air, the transition from partial slip to gross slip was seen for higher amplitudes above 10 nm, but in water the amplitude reaches only 7 nm.

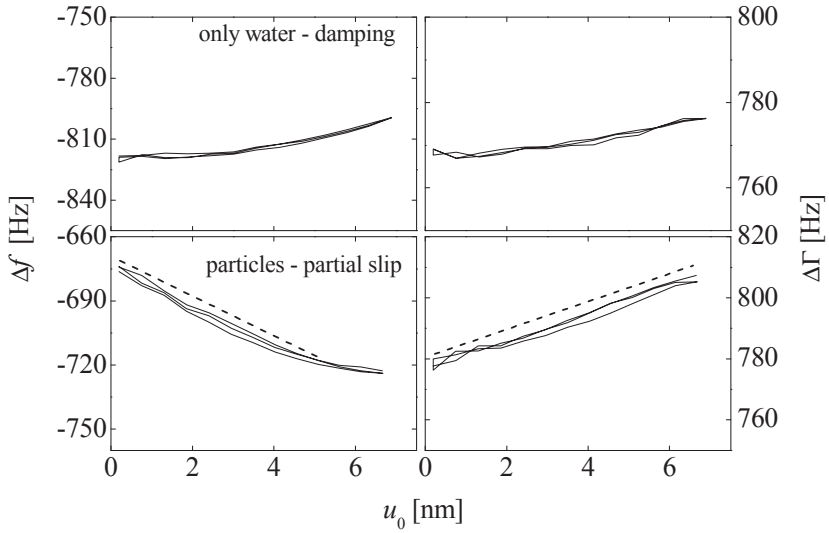

Fig. 24 Measurements in water (2 mm particles on silica surface)

Two models for partial slip were described – Cattaneo-Mindlin and Savkoor. For all data the Cattaneo-Mindlin model fits better than Savkoor model. This also corresponds with the previous result in Ref.[20]. The agreement with Cattaneo-Mindlin is interesting, because this model assumes standard macroscopic friction in the sliding zone, but the contact area is in micro-scale range. The explanation is not clear, probably the nanoroughness plays a role.[32]

In some measurements the plateau occurs at small amplitudes. This corresponds to the linear behaviour of viscoelastic contact. The transition from viscoelastic behaviour to partial slip is also discussed in Ref.[33] The plateau occurs because the tangential stress in the contact without slip never go to infinity in real contacts due to a ring-shape region close to the edge.[32]

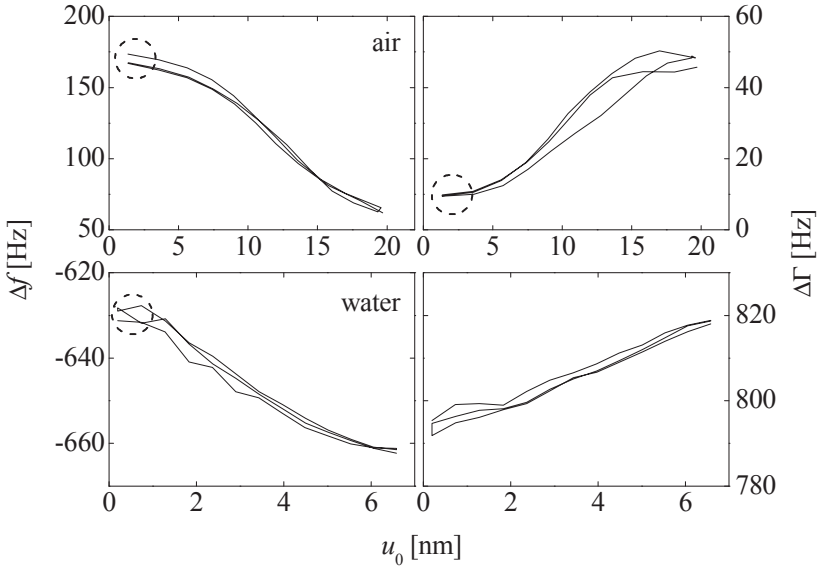

Fig. 25 Plateau (2 mm particles on silica surface)

4.2 Application of Cattaneo-Mindlin model for partial slip

As an example of data evaluating (Fig. 26), 2 mm particles on silica surface in water was chosen. The dependence of frequency shift on amplitude of motion was measured for varied mass *m*. From these data, the offset and the slope were taken. In order to obtain the slope, some of the first and last values had to be discarded because of plateau. Following equations 19 of Cattaneo-Mindlin model, the contact stiffness was calculated from the offset.

$$\begin{aligned} \Delta f(u_0) &= \frac{n_p}{2n\pi^2 A_{eff} Z_q}\kappa - \frac{n_p}{2n\pi^2 A_{eff} Z_q}\frac{\kappa^2}{3\mu F_\perp}u_0 \\ offset_{\Delta f} &= \frac{n_p}{2n\pi^2 A_{eff} Z_q}\kappa \\ \kappa &= offset_{\Delta f}\frac{2n\pi^2 A_{eff} Z_q}{n_p} \end{aligned} \tag{24}$$

Using the contact stiffness, the contact radius was calculated according to equations 16, 17, 21 and plotted against mass *m*. The values of *E* and ν for the calculation were estimated as *E* = 70 GPa and ν = 0.17.[38] These values are for fused silica, the thin layer on the surface was neglected.

From slopes, two friction coefficients were calculated and plotted against mass *m*. The first friction coefficient $\mu_{\Delta f}$ was calculated from the slope of dependence of Δf on u_0.

$$\begin{aligned} \Delta f(u_0) &= \frac{n_p}{2n\pi^2 A_{eff} Z_q}\kappa - \frac{n_p}{2n\pi^2 A_{eff} Z_q}\frac{\kappa^2}{3\mu F_\perp}u_0 \\ slope_{\Delta f} &= \frac{n_p}{2n\pi^2 A_{eff} Z_q}\frac{\kappa^2}{3\mu F_\perp} \\ \mu_{\Delta f} &= \frac{1}{slope_{\Delta f}}\frac{n_p}{2n\pi^2 A_{eff} Z_q}\frac{\kappa^2}{3F_\perp} \end{aligned} \tag{25}$$

The second friction coefficient $\mu_{\Delta\Gamma}$ was calculated from theslope of dependence of $\Delta\Gamma$ on u_0.

$$\begin{aligned} \Delta\Gamma(u_0) &= \Delta\Gamma_{off} + \frac{n_p}{2n\pi^2 A_{eff} Z_q}\frac{4}{9\pi}\frac{\kappa^2}{\mu F_\perp}u_0 \\ slope_{\Delta\Gamma} &= \frac{n_p}{2n\pi^2 A_{eff} Z_q}\frac{4}{9\pi}\frac{\kappa^2}{\mu F_\perp} \\ \mu_{\Delta\Gamma} &= \frac{1}{slope_{\Delta\Gamma}}\frac{n_p}{2n\pi^2 A_{eff} Z_q}\frac{4}{9\pi}\frac{\kappa^2}{F_\perp} \end{aligned} \tag{26}$$

As it was stated in chapter 2.3.1, these friction coefficients should be equal in Cattaneo-Mindlin model, this means their ratio should be 1.

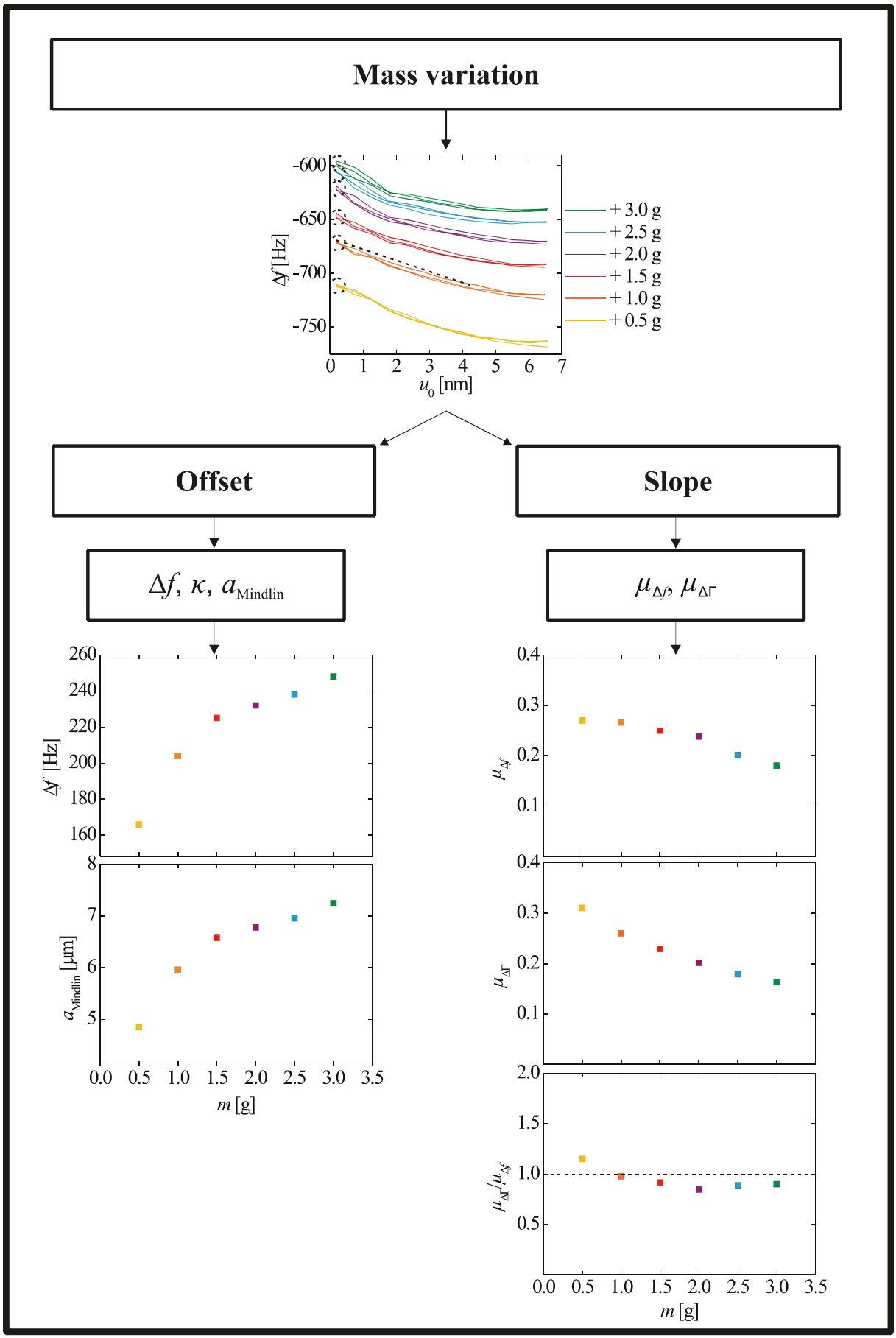

Fig. 26 Evaluation procedure

The evaluation was carried out for nine measurements which were performed under the same conditions – crystal surface, particle size and environment e.g. a total of nine measurements of 2 mm particles on silica surface in water. The graphs are included in the appendix.

These nine curves were averaged and compared with other measurements which were performed under varied conditions as given in Tab. 1 in chapter 3.2.4.

4.3 Application of models for dependence of contact radius on the normal force

The curves of Δf and a depend on u_0 obtained with the previous procedure were compared with standard contact models. At first the Hertz, model was applied. For calculation of contact radius predict by Hertz (equation 1), the values of E and ν were estimated like in the previous chapter. Fig. 27 shows that there are substantial discrepancies between the experimental data and the Hertz model.

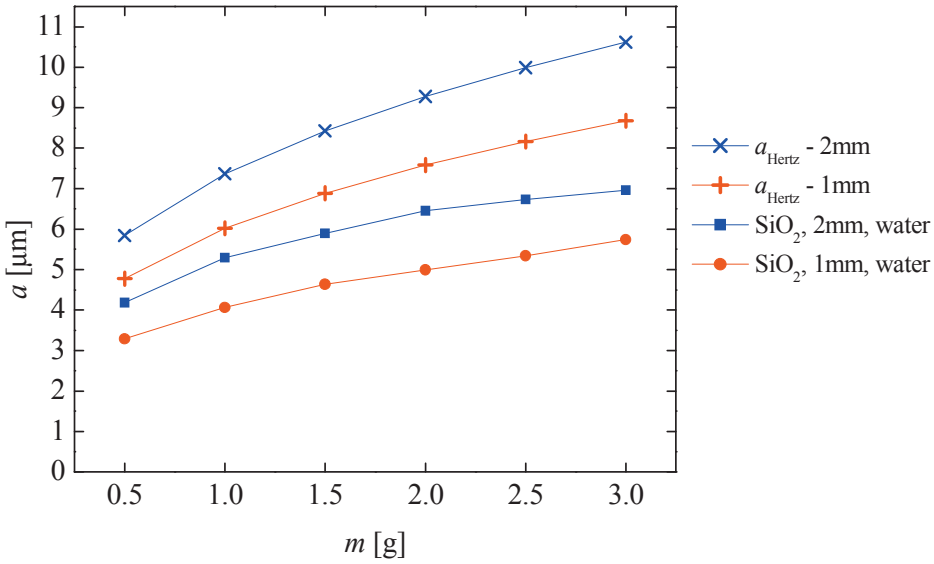

Fig. 27 Comparison with Hertz model

The next step was applying JKR model on the experimental data (Fig. 28). For these calculations, not the contact radius but the value of the frequency shift at low amplitude (offset) was taken. There is no difference in the shape of curves because Δf is directly proportional to a. By fitting the JKR function to the dependence of Δf on applied mass, the parameters E^* and γ were obtained as fit parameters.

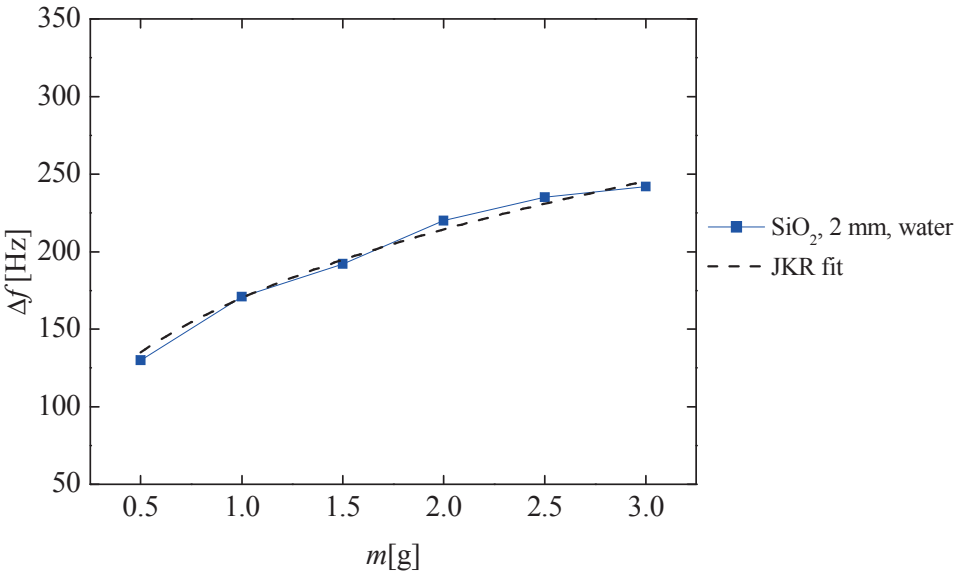

Fig. 28 Fitting by JKR model

All nine curves were fitted by JKR and nine values for the parameters E^* and γ were obtained. The mean values for E^* and γ were calculated (Tab. 2). The same procedure was used for five other measured combinations (Tab. 1). In other words, six mean values of E^* and γ were obtained for all varied combinations. The values confirm the first estimation of E^* = 70 GPa. There is considerable scatter, but still both parameters E^* and γ are in the expected range.

Tab. 2 Means values of E^* and γ and their standard deviations

Surface	Particles diameter [mm]	Environment	E^* [GPa]	γ[N/m]
SiO_2	2.2	Air	106.8 ± 33.8	0.246 ± 0.218
SiO_2	2.2	Water	76.7 ± 36.5	0.159 ± 0.157
SiO_2	1.2	Air	67.3 ± 16.7	0.127 ± 0.199
SiO_2	1.2	Water	60.1 ± 22.2	0.205 ± 0.279
PMMA	2.2	Air	77.4 ± 31.4	0.035 ± 0.047
PMMA	2.2	Water	61.3 ± 24.6	0.068 ± 0.130

4.4 Comparison of results obtained under varied conditions

The following results were obtained by averaging of nine curves of experiments performed under the same conditions. In this chapter, the dependences of Δf, $\mu_{\Delta f}$, $\mu_{\Delta\Gamma}$ and ratio of $\mu_{\Delta f}$ and $\mu_{\Delta\Gamma}$ on applied mass will be discussed and compared with measurement which were performed under varied condition (Tab. 1, chapter 3.2.4).

4.4.1 Contact radius

Fig. 29 depictes the dependence of Δf at low amplitude on applied mass. The frequency shift of 1 mm particles is smaller than the one obtained with 2 mm particles. This was expected because the contact radius of a sphere with 1mm diameter should be smaller than that of a sphere of 2 mm. The Δf of 2 mm spheres on silica surface and PMMA are similar under smaller load. Under larger load, the increase in Δf for spheres on PMMA surface is slightly higher than for silica surface. The polymer surface is softer than silica surface. Under larger load, the spheres on PMMA could go deeper into the polymer layer, thereby the contact radius is larger. It also might be influence of averaging, because the measurements on PMMA showed worse reproducibility, which was presumably caused by hydrophobicity of PMMA.

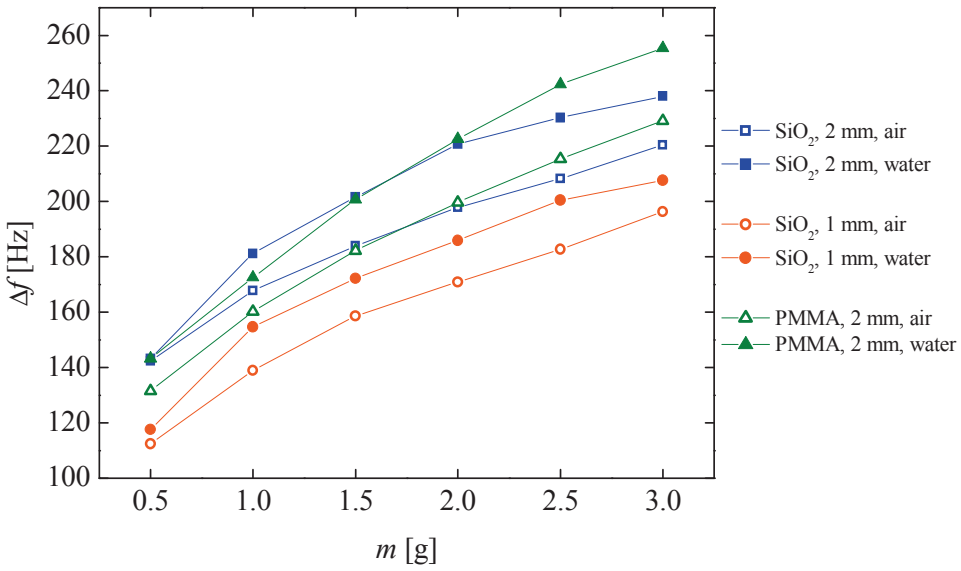

Fig. 29 Dependence of frequency shift on applied mass for varied combinations (without standard deviations for better clarity)

In Fig. 29, the error bars were discarded for better clarity. Fig. 30 shows separated curves with error bars which represent standard deviations of means values.

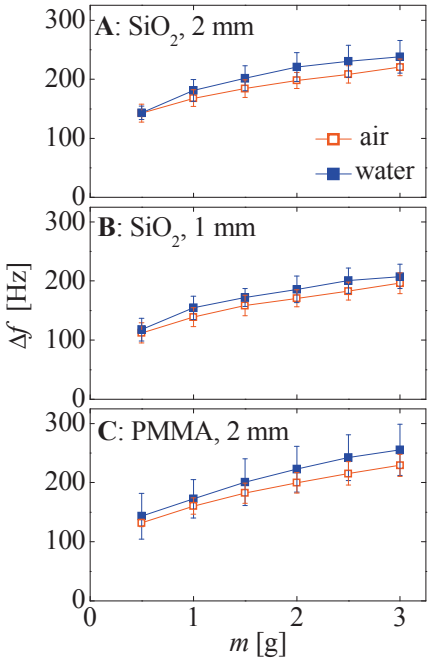

Fig. 30 Dependence of frequency shift on applied mass for varied combinations with standard deviations

The most surprising result has been a higher frequency shift in water than in air for corresponding measurements. The expectation was higher Δf in air as a consequence of an effect of capillary forces which have no influence in water. The explanation of higher frequency shift in water is not clear. The possible explanation is illustrated in Fig. 31. Because of high-frequency oscillations (5 MHz), the contact is rolling but water cannot be squeezed out of place closed to the contact area and it leads to an apparent increase in the contact area. At this point, there is not a detailed model, which would support this hypothesis.

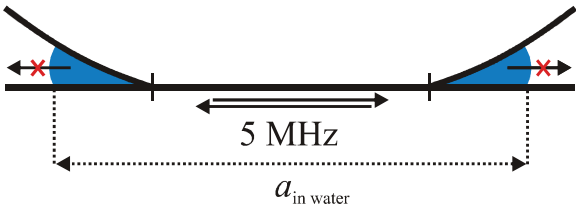

Fig. 31 A sketch of how a squeeze flow of water at the edge of a contact might increases the effective contact stiffness, when measured at 5 MHz

4.4.2 Friction coefficient

The dependence of $\mu_{\Delta f}$ and $\mu_{\Delta\Gamma}$ on applied mass displays downward curves (Fig. 32 and Fig. 33). For the explanation, the measured friction coefficient is viewed as an apparent friction coefficient μ_{app}, which is defined as

$$\mu_{app} = \frac{F_{\parallel}}{F_{ext}} \tag{27}$$

The F_{ext} is the external normal force – in this case the added weight. The F_{ext} together with the adhesive force F_{adh} is a part of total normal load $F_{\perp tot.}$ (equation 28). The F_{adh} is shown in equation 6.

$$F_{\perp tot.} = F_{ext} + F_{adh} \tag{28}$$

The relation between the real friction coefficient μ and the measured apparent friction coefficient μ_{app} is derived from Amontons' law of friction.

$$\begin{aligned} F_{\parallel} &= \mu F_{\perp} \\ F_{\parallel} &= \mu\left(F_{ext} + F_{adh}\right) \\ F_{\parallel} &= \mu F_{ext}\left(1 + \frac{F_{adh}}{F_{ext}}\right) \\ \frac{F_{\parallel}}{F_{ext}} &= \mu\left(1 + \frac{F_{adh}}{F_{ext}}\right) \\ \mu_{app} &= \mu\left(1 + \frac{F_{adh}}{F_{ext}}\right) \end{aligned} \tag{29}$$

If the condition of $F_{adh} < F_{ext}$ is met, the increase in F_{ext} causes decrease in μ_{app}.

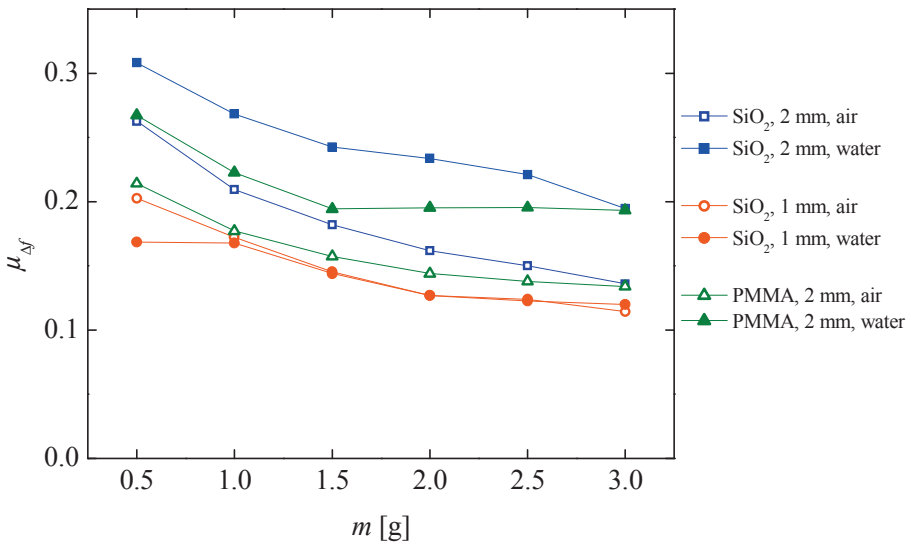

Fig. 32 Dependence of friction coefficient from frequency shift on applied mass for varied combinations (without standard deviations for better clarity)

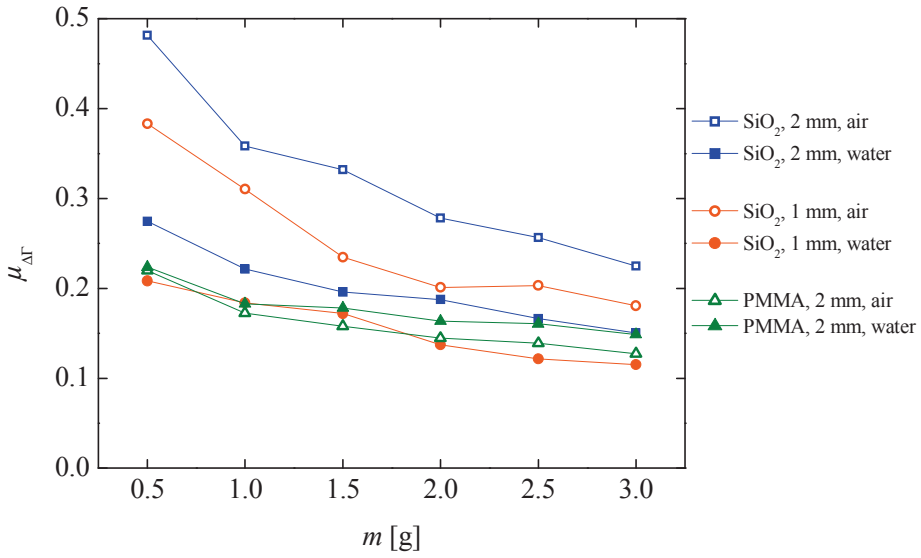

Fig. 33 Dependence of friction coefficient from bandwidth shift on applied mass for varied combinations (without standard deviations for better clarity)

Fig. 34 shows the dependence of ration of $\mu_{\Delta f}$ and $\mu_{\Delta\Gamma}$ on applied mass. As described before, this ratio, according Cattaneo-Mindlin model, should be 1. The values of the ratios are nearly constant or slightly decreasing around 1 except for measurements for spheres of 2 mm and 1 mm diameter on silica surface in air. Values of these ratios lie around 1.7. This is caused by $\mu_{\Delta\Gamma}$, which is for both types of measurement very high, in opposition to $\mu_{\Delta f}$. This could be caused by other interface processes of dissipation which may be related to capillary forces.

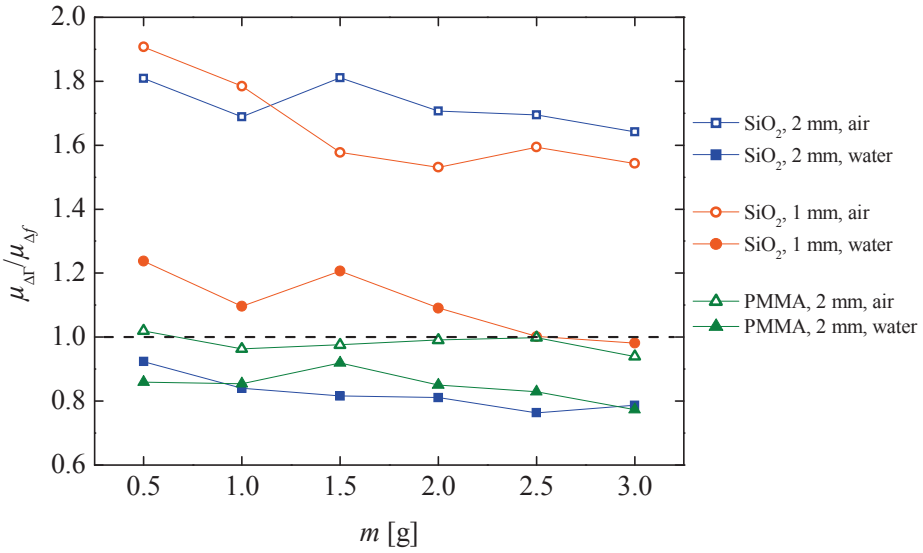

Fig. 34 Dependence of ratio of friction coefficients on applied mass for varied combinations (without standard deviations for better clarity)

As well as in the case of comparison of contact radii, the error bars were discarded from Fig. 32, Fig. 33 and Fig. 34 for better clarity. Fig. 35 shows separated curves with the error bars which represent the standard deviations of the means values.

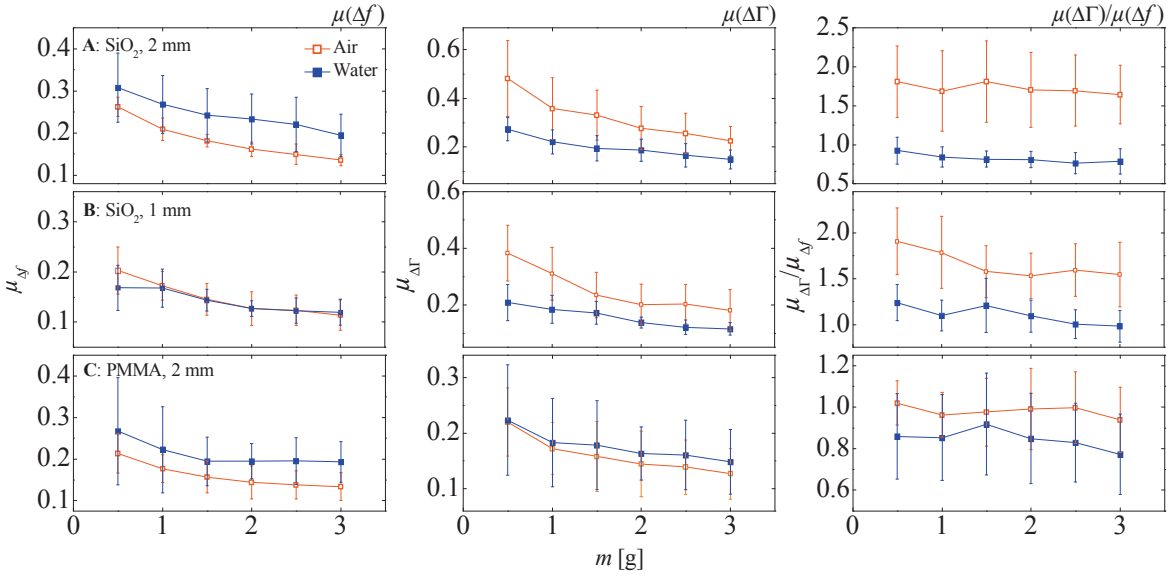

Fig. 35 Dependence of friction coefficients and their ratio on applied mass for varied combinations with standard deviations

4.5 Evaluation of shake-down and shake-up

Through experiments, which are described in chapter 3.2.5, the dependences of ΔΓ on the time *t* for varied amplitude were obtained. The aim of this evaluation was to find out the occurrence of shake-down and shake-up, in other words, to determine which of these phenomena is observed more often. For explanation of data evaluation, one example of experiment was taken (2 mm sphere on silica surface in water loaded by 3.0 g). For increasing amplitude, the slope of dependences of ΔΓ on the time was taken (Fig. 36).

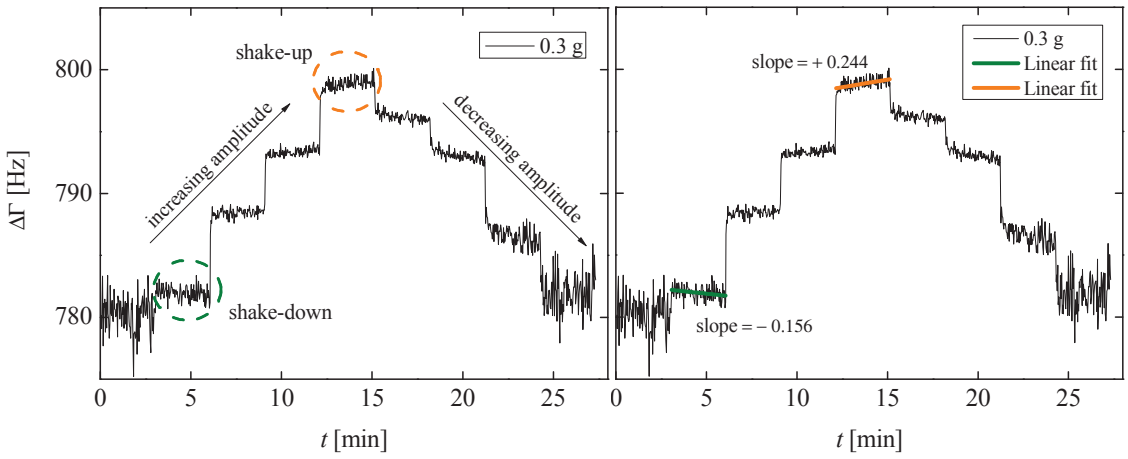

Fig. 36 Measurements of dependence of ΔΓ on the time for varied amplitude

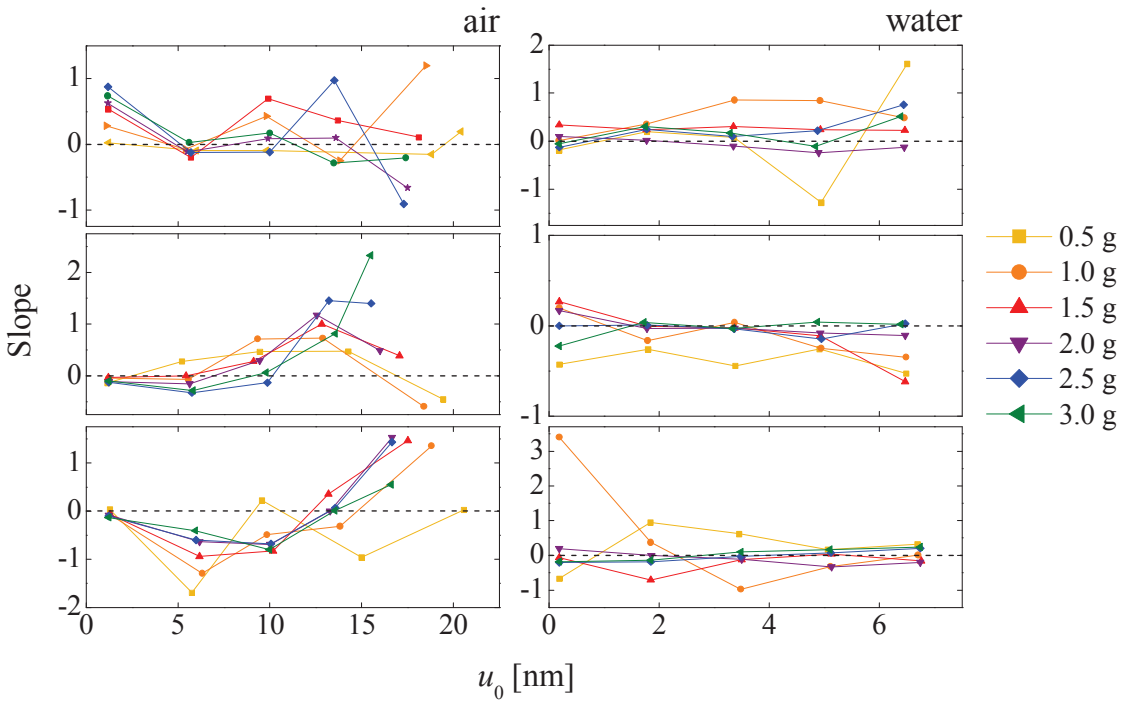

Fig. 37 Occurrence of shake-down (points under dashed line) and shake-up (points above dashed line)

The measurement performed with 2 mm particles on silica surface in air and water show that both phenomena occur equally often. It does not correspond with previous observing. A previous experiment for smaller particles in the air showed more often shake-down than shake-up.[32] An explanation for this behaviour was not found.

5 CONCLUSION

The current thesis focused on sphere-plate contact in water studied with high frequency shear oscillations. Under this condition, the sphere-plate contact undergoes partial slip. The Cattaneo-Mindlin model was applied on results obtained because it fits better than the Savkoor´s. From the point of view of Cattaneo-Mindlin model, the contact radius and the friction coefficient were calculated.

The measurements of these contacts were performed in air and in water and, from their comparison, differences were determined. In case of air as the environment, the partial slip traversed to the gross slip at an amplitude of 10 nm for load 0.5 g and 1.0 g. At higher loads the gross slip was not observed. On the contrary, in water as an environment, the transition from partial slip to gross slip was not seen due to damping of oscillation; the oscillation reached only 7 nm and that was not likely to be sufficient for gross slip.

Appling the Cattaneo-Mindlin model, the friction coefficients from frequency shift and bandwidth shift were calculated. It was found that the friction coefficient decreases in relation to an increase in applied mass. This behaviour can be explained with an adhesive force contributing to the total normal force. This causes that the apparent friction coefficient is inversely proportional to external forces (equation 29).

The ratio of $\mu_{\Delta f}$ and $\mu_{\Delta\Gamma}$ should be equal to 1 according to Cattaneo-Mindlin model. This condition is approximately fulfilled in four cases. However, for the case of silica surface, these ratios lie around 1.7. In this case the other interface processes of dissipation as a capillary forces come into play.

The calculated contact radius was compared with JKR and Hertz models. The comparison showed that JKR model corresponded better than Hertz model. Fitting by JKR to dependence of contact radius on applied mass, E^* and γ were obtained as fit parameters. Both parameters E^* and γ were in the expected range.

The comparison of averaged contact radii, which were measured under varied conditions, showed a larger contact radius in water than in air. The explanation is not clear, although a possible hypothesis is mentioned in chapter 4.4.1.

The measurements for 2 mm particles were performed on two different surfaces. One was a hydrophilic SiO_2 surface and the second a hydrophobic PMMA surface. Variation of these surfaces did not have a distinctive influence on measurements. Nevertheless, the samples measured on PMMA surface in water showed worse reproducibility because of the repulsion between water and hydrophobic surface.

In order to find shake-down and shake-up, additional experiments were carried out. These experiments shows that occurrence of shake-down and shake-up is observed equally often. This result is in discrepancy with previous results and it necessary to perform other experiments in future research.

In long-term perspective, these findings could be useful for studies of attachment and detachment of cells on the surface and their possible detection by QCM.

6 LITERATURE

[1] POPOV, V. L. *Contact Mechanics and Friction. Physical Principles and Applications:* Springer Berlin Heidelberg, 2010. 978-3-642-10802-0.

[2] JOHNSON, K. L. *Contact Mechanics.* 9th ed.: Cambridge University Press, 1987. 9780521347969.

[3] FISCHER-CRIPPS, A. C. *Introduction to Contact Mechanics.* 2nd ed.: Springer US, 2007. 978-0-387-68187-0.

[4] KATTA, J., Z. JIN, E. INGHAM, and J. FISHER. Biotribology of articular cartilage - A review of the recent advances [online]. *Medical Engineering & Physics.* 2008, 30(10), 1349-1363 [viewed 31 March 2014, 12:00]. Available from: 10.1016/j.medengphy.2008.09.004.

[5] RMAILE, A., D. CARUGO, L. CAPRETTO, X. ZHANG, J. A. WHARTON, P. J. THURNER, M. ASPIRAS, M. WARD, and P. STOODLEY. Microbial tribology and disruption of dental plaque bacterial biofilms [online]. *Wear.* 2013, 306(1-2), 276-284. Available from: 10.1016/j.wear.2013.02.010.

[6] KAMPERMAN, M., E. KRONER, A. DEL CAMPO, R. M. MCMEEKING, and E. ARZT. Functional Adhesive Surfaces with "Gecko" Effect: The Concept of Contact Splitting [online]. *Advanced Engineering Materials.* 2010, 12(5), 335-348. Available from: 10.1002/adem.201000104.

[7] BHUSHAN, B. Gecko Feet: Natural Hairy Attachment Systems for Smart Adhesion – Mechanism, Modeling and Development of Bio-Inspired Materials. *Nanotribology and Nanomechanics:* Springer Berlin Heidelberg, 2008, pp. 1073-1134.

[8] ERITEN, M., A. A. POLYCARPOU, and L. A. BERGMAN. Physics-based modeling for partial slip behavior of spherical contacts [online]. *International Journal of Solids and Structures.* 2010, 47(18–19), 2554-2567. Available from: 10.1016/j.ijsolstr.2010.05.017.

[9] HERTZ, H. Ueber die Berührung fester elastischer Körper [online]. *Journal für die reine und angewandte Mathematik.* 1882, 1882(92), 156-171. Available from: 10.1515/crll.1882.92.156.

[10] BRADLEY, R. S. LXXIX. The cohesive force between solid surfaces and the surface energy of solids [online]. *Philosophical Magazine Series 7.* 1932, 13(86), 853-862. Available from: 10.1080/14786449209461990.

[11] JOHNSON, K. L., K. KENDALL, and ROBERTS, A. D. Surface Energy and the Contact of Elastic Solids [online]. *Proceedings of the Royal Society of London. Series A, Mathematical and Physical Sciences.* 1971, 324(1558), 301-313. Available from: 10.2307/78058.

[12] DERJAGUIN, B. V., V. M. MULLER, and Yu. P. TOPOROV. Effect of contact deformations on the adhesion of particles [online]. *Journal of Colloid and Interface Science.* 1975, 53(2), 314-326. Available from: 10.1016/0021-9797(75)90018-1.

[13] TABOR, D. Surface forces and surface interactions [online]. *International Conference on Colloids and Surfaces.* 1977, 58(1), 2-13. Available from: 10.1016/0021-9797(77)90366-6.

[14] MAUGIS, D. Adhesion of spheres: The JKR-DMT transition using a Dugdale model [online]. *Journal of Colloid and Interface Science.* 1992, 150(1), 243-269. Available from: 10.1016/0021-9797(92)90285-T.

[15] BHUSHAN, B. *Handbook of Micro/Nano Tribology, Second Edition:* Taylor & Francis, 1998. 9780849384028.

[16] HEYDENREICH, L. H., B. DIBNER, and L. RETI. *Leonardo, der Erfinder:* Wiss. Buchges, 1985.

[17] BAUMBERGER, T. Dry Friction Dynamics at Low Velocities. In: B.N.J Persson and E. Tosatti, eds. *Physics of Sliding Friction:* Springer Netherlands, 1996, pp. 1-26.

[18] PERSSON, BO N. J. Sliding on Lubricated Surfaces. *Sliding Friction:* Springer Berlin Heidelberg, 2000, pp. 101-170.

[19] Crystal Notes. JAUCH QUARTZ GMBH. *Jauch quartz GmbH Products: quartz crystal, oscillator, filter, ceramic resonator.* [online].[2014-05-04]. Available from: http://www.jauch.de/pages/de_crystal_notes.php5.

[20] HANKE, S. *Untersuchungen zur Mikrotribologie unter Hochfrequenter Oszillatorischer Anregung.* Clausthal, 2013. Dissertation. Clausthal University of Technology.

[21] LAUGHLIN, R. B. Introduction to Quartz Crystal Microbalance [online]. In: *Prof. Robert B. Laughlin, Department of Physics, Stanford University*[online]. 2007 [2014-04-14]. Available from: http://large.stanford.edu/courses/2007/ph210/hellstrom2/.

[22] JOHANNSMANN, D. Studies of Viscoelasticity with the QCM. In: Andreas Janshoff and Claudia Steinem, eds. *Piezoelectric Sensors:* Springer Berlin Heidelberg, 2007, pp. 49-109.

[23] SAUERBREY, G. Verwendung von Schwingquarzen zur Wägung dünner Schichten und zur Mikrowägung [online]. *Zeitschrift für Physik.* 1959, 155(2), 206-222. Available from: 10.1007/BF01337937.

[24] FINGER, A. *Formation and Characterization of Nanobubbles with an Electrochemical Quartz Crystal Microbalance.* Clausthal, 2012. Dissertation. Clausthal University of Technology.

[25] KANAZAWA, K. K., and J. G. GORDON. Frequency of a quartz microbalance in contact with liquid [online]. *Anal. Chem.* 1985, 57(8), 1770-1771. Available from: 10.1021/ac00285a062.

[26] REED, C. E., KANAZAWA, K. KEIJI, and J. H. KAUFMAN. Physical description of a viscoelastically loaded AT-cut quartz resonator [online]. *Journal of Applied Physics.* 1990, 68(5), 1993-2001. Available from: 10.1063/1.346548.

[27] BECKER, B., and M. A. COOPER. A survey of the 2006–2009 quartz crystal microbalance biosensor literature [online]. *Journal of Molecular Recognition.* 2011, 24(5), 754-787. Available from: 10.1002/jmr.1117.

[28] JOHANNSMANN, D. Studies of Contact Mechanics with the QCM. In: Andreas Janshoff and Claudia Steinem, eds. *Piezoelectric Sensors:* Springer Berlin Heidelberg, 2007, pp. 151-170.

[29] DYBWAD, G. L. A sensitive new method for the determination of adhesive bonding between a particle and a substrate [online]. *Journal of Applied Physics.* 1985, 58(7), 2789-2790. Available from: 10.1063/1.335874.

[30] MINDLIN, RAYMOND D., DERESIEWICZ, HERBERT. Elastic Spheres in Contact under Varying Oblique Forces. *Journal of Applied Mechanics -Transactions of the Asme.* 1953, 20(3), 327-344.

[31] SAVKOOR, A. R. *Dry adhesive friction of elastomers. A study of the fundamental mechanical aspects.* Delft, 1987. Dissertation. Delft University of technology.

[32] HANKE, S., J. PETRI, and D. JOHANNSMANN. Partial slip in mesoscale contacts: Dependence on contact size [online]. *Physical Review E.* 2013, 88(3), 32408. Available from: http://link.aps.org/doi/10.1103/PhysRevE.88.032408.

[33] LÉOPOLDÈS, J., and X. JIA. Transverse Shear Oscillator Investigation of Boundary Lubrication in Weakly Adhered Films [online]. *Physical Review Letters.* 2010, 105(26), 266101. Available from: http://link.aps.org/doi/10.1103/PhysRevLett.105.266101.

[34] MELAN, E. Zur plastizität des räumlichen kontinuums. *Ingenieur-Archiv.* 1938, IX, 116-126.

[35] KLARBRING, A., M. CIAVARELLA, and J. R. BARBER. Shakedown in elastic contact problems with Coulomb friction [online]. *International Journal of Solids and Structures.* 2007, 44(25–26), 8355-8365. Available from: 10.1016/j.ijsolstr.2007.06.013.

[36] GOOCH, J. W., ed. *Encyclopedic Dictionary of Polymers:* Springer New York, 2007. 978-0-387-31021-3.

[37] BRANDRUP, J. , IMMERGUT, E. H. *Polymer Handbook.* New York: J. Wiley, 1989. 0471812447.

[38] CALLISTER, W. D. and D. G. RETHWISCH. *Fundamentals of Materials Science and Engineering: An Integrated Approach:* Wiley, 2012. 9781118061602.

7 LIST OF ABBREVIATIONS

e.g.	for example
Fig.	Figure
JKR	Johnson, Kendall and Roberts
PMMA	poly(methyl metacrylate)
SLA	small load approximation
QCM	quartz crystal microbalance

8 LIST OF SYMBOLS

a	contact radius
a_{Hertz}	contact radius according to Hertz model
a_{JKR}	contact radius according to JKR model
$a_{Mindlin}$	contact radius according to Cattaneo-Mindlin model
A_{eff}	effective area of quartz crystal
c_q	speed of sound of quartz
d	penetration depth
d_q	thickness of the quartz crystal
E	Young's modulus (elastic modulus)
E^*	effective Young's modulus
f	resonance frequency
f_F	fundamental frequency
$F_\perp$	normal force
$F_{\perp tot.}$	total normal force
$F_\parallel$	tangential force
F_A	pull-off force
F_{adh}	adhesive force
F_{ext}	external force
F_k	kinetic friction
F_s	static friction
G	shear modulus
G^*	effective shear modulus
m	mass
n	order of overtone
n_p	number of spheres
p	distribution of normal stress
p_0	normal stress in the centre of contact area
r	distance from centre of contact area
R_P	radius of sphere
t	time
T_g	glass transition temperature
u_0	amplitude of oscillation

u_{cr}	critical amplitude
Z_q	acoustic impedance of the quartz
Δd	thickness of the film deposited on quartz
Δf	frequency shift
$\Delta\Gamma$	bandwidth shift
Γ	bandwidth (half-width at half-maximum of the resonance frequency)
γ	surface energy
ε	strain
κ	contact stiffness
λ	wavelength
μ	friction coefficient
μ_{app}	apparent friction coefficient
μ_k	kinetic friction coefficient
μ_s	static friction coefficient
$\mu_{\Delta f}$	friction coefficient calculated from frequency shift
$\mu_{\Delta\Gamma}$	friction coefficient calculated from bandwidth shift
ν	Poisson's ratio
σ	stress
$\sigma_\perp$	normal stress
$\sigma_\parallel$	tangential stress
ρ_f	density of deposited film
τ_0	Tresca friction ($\tau_0 = 0$)

9 APPENDIX

Dependence of frequency shift at low amplitude on the applied mass

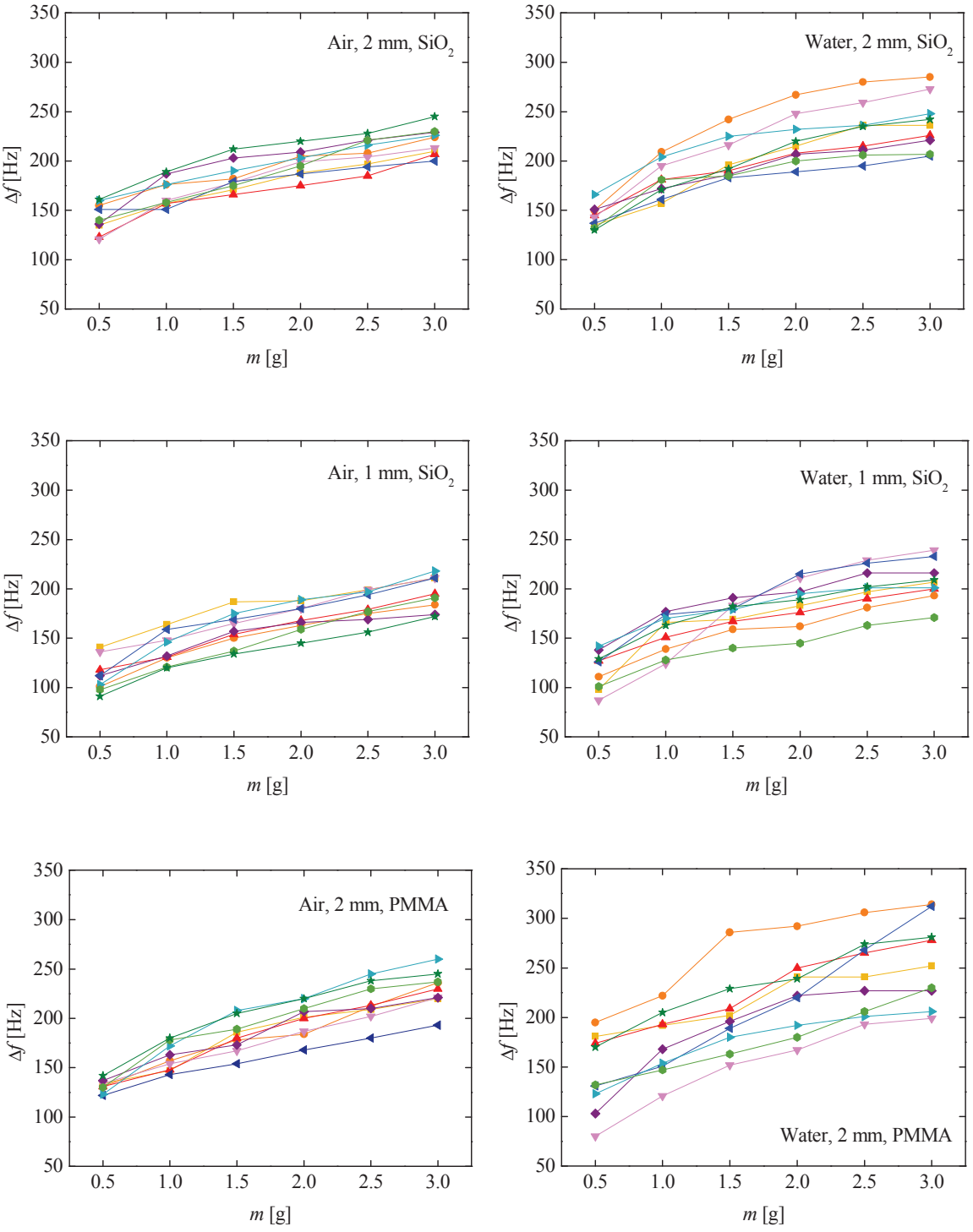

Dependence of friction coefficient calculated from frequency shift on the applied mass

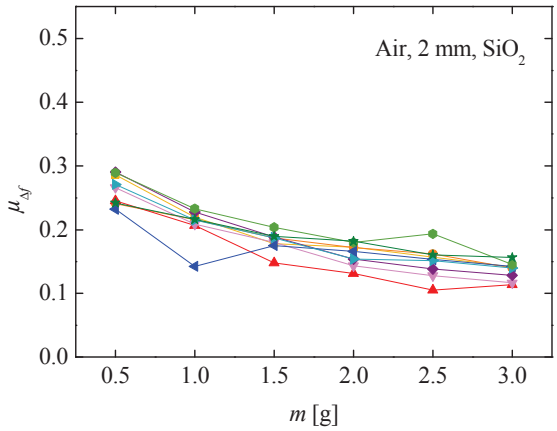

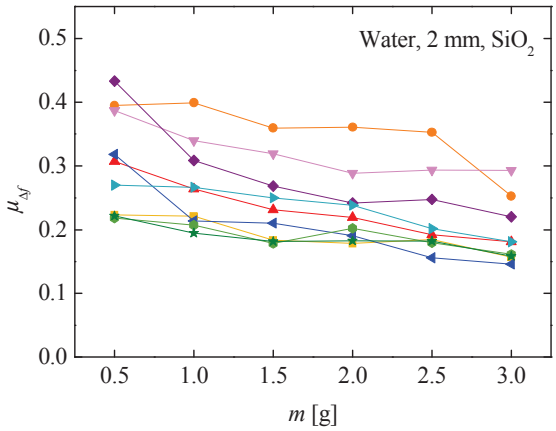

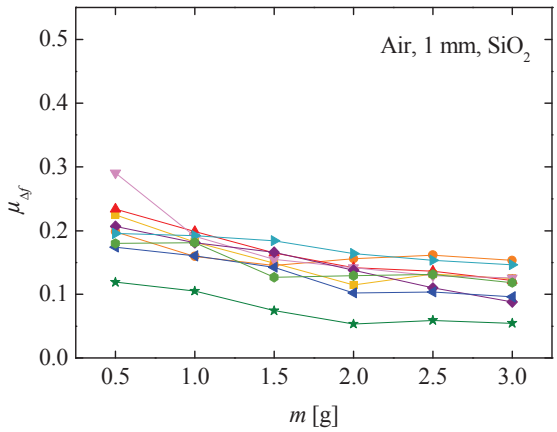

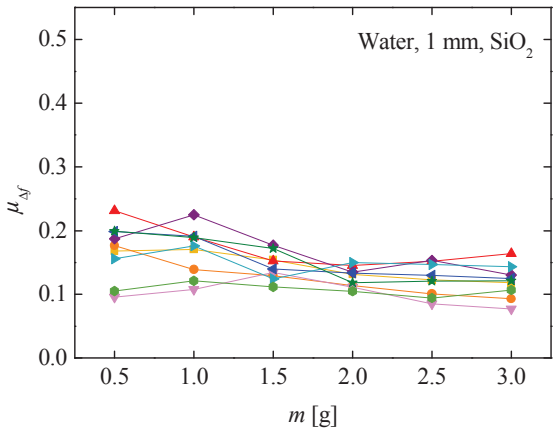

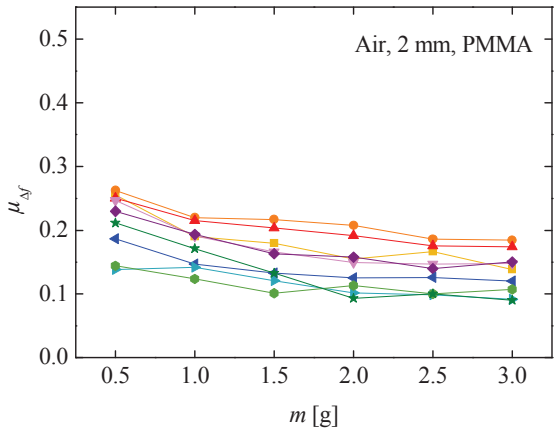

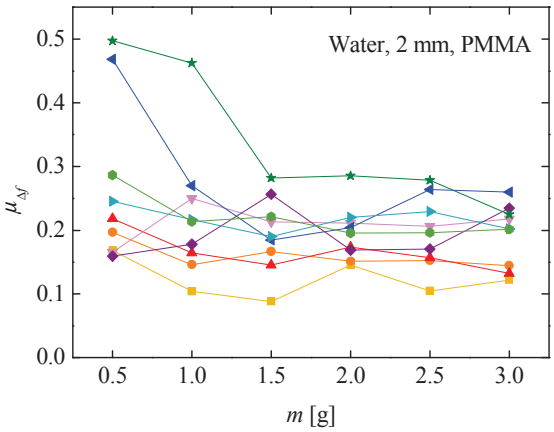

Dependence of friction coefficient calculated from bandwidth shift on the applied mass

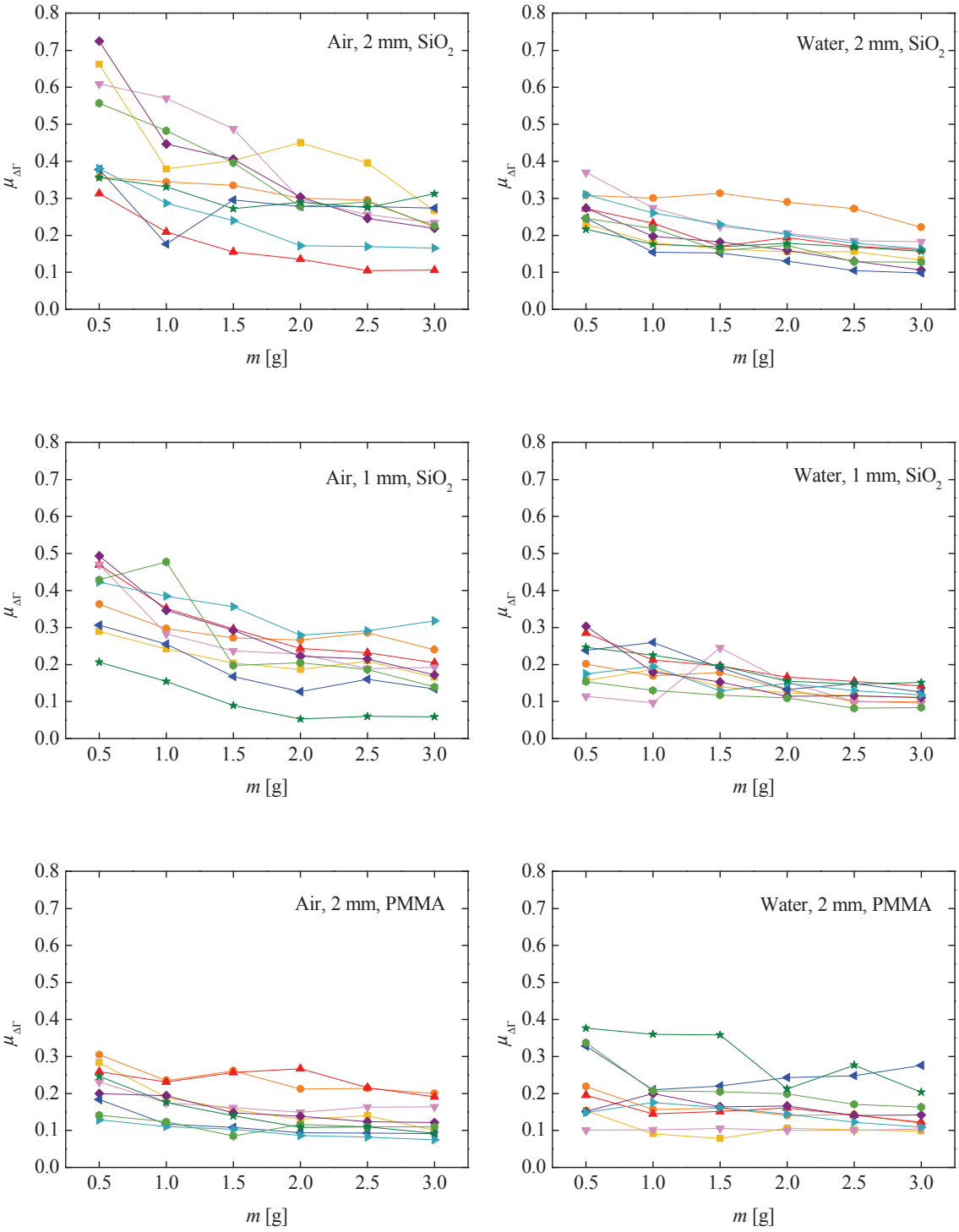

Dependence of friction coefficients on the applied mass